



HAL
open science

Reconstruction of the Holocene Climate and Environmental changes of Niayes Peat Bog in Northern coast of Senegal (NW Africa) based on Stable Isotopes and Charcoals Analysis

Ada Ndiaye, Ilham Bentaleb, Charly Favier, François Fourel, David Sebag, Mamadou Fall, Pierre Giresse, Bachir Diouf

► To cite this version:

Ada Ndiaye, Ilham Bentaleb, Charly Favier, François Fourel, David Sebag, et al.. Reconstruction of the Holocene Climate and Environmental changes of Niayes Peat Bog in Northern coast of Senegal (NW Africa) based on Stable Isotopes and Charcoals Analysis. *Quaternary Science Reviews*, 2022, 289, pp.107609. 10.1016/j.quascirev.2022.107609 . hal-03718018

HAL Id: hal-03718018

<https://ifp.hal.science/hal-03718018v1>

Submitted on 8 Jul 2022

HAL is a multi-disciplinary open access archive for the deposit and dissemination of scientific research documents, whether they are published or not. The documents may come from teaching and research institutions in France or abroad, or from public or private research centers.

L'archive ouverte pluridisciplinaire **HAL**, est destinée au dépôt et à la diffusion de documents scientifiques de niveau recherche, publiés ou non, émanant des établissements d'enseignement et de recherche français ou étrangers, des laboratoires publics ou privés.

Reconstruction of the Holocene Climate and Environmental Changes of Niayes Peat Bog in Northern Coast of Senegal (NW Africa) Based on Stable Isotopes and Charcoals Analysis.

Ada Ndiaye ^{a, b, *}, Ilham Bentaleb ^b, Charly Favier ^b, François Fourel ^c, David Sebag ^{d, e}, Mamadou Fall ^a, Pierre Giresse ^f, Bachir Diouf ^a

a. Département de Géologie, FST, UCAD, BP 5005 Dakar-Fann, Sénégal

b. ISE-M, UMR 5554, Université de Montpellier, Montpellier, France

c. LEHNA, UMR 5023, Université de Claude Bernard Lyon 1, Villeurbanne, France

d. IFP Energies Nouvelles, Earth Sciences and Environmental Technologies Division, 1 et 4 avenue de Bois-Préau 92852 Rueil-Malmaison, France

e. Institute of Earth Surface Dynamics, Geopolis, University of Lausanne, Lausanne, Switzerland

f. CEFREM, UMR 5110, Université de Perpignan, Perpignan, France

Corresponding Author:

Ada Ndiaye

Université Cheikh Anta Diop – Faculté des Sciences et Techniques

Département de Géologie – BP 5005 Dakar-Fann Sénégal

Tél. (+221) 77 557 47 18

Email : ada.ndiaye@ucad.edu.sn

Funding: This research was supported by the PAES project-UEMOA-West Africa (grant number 2100155007376); and the Project South IRD-ISE-Montpellier.

Highlights

- The $\delta^{13}\text{C}$ decrease between 9.4 and 5.5 cal kyr BP shows that the African Humid Period (AHP) was a time of increased humidity in the northern coast of Senegal as across West Africa.
- The low charcoal influx, the high W/L ratios and the low human density during the AHP indicate weak natural forest fires, likely caused by lightning.
- After 5.5 cal kyr BP, the $\delta^{13}\text{C}$ increase shows a dry late Holocene but interrupted by two Little Humid Periods (LHP).
- The high charcoal influx, the low W/L ratio and the high human density indicate an anthropogenic savanna fires activation during the Late Holocene.

1 **Abstract**

2 A core from a peat bog in the “Niayes” region, northwest of Senegal, provides a valuable insight
3 into the evolution of the landscape and fire regime related to the West African Monsoon rainfall
4 and to human impact over the Holocene. The high-resolution multiproxy approach based on
5 stable carbon isotopic composition ($\delta^{13}\text{C}$), Rock-Eval[®] thermal analysis, and charcoal analysis,
6 provides an understanding of vegetation composition (C_3/C_4) and fire regime in the continental
7 watershed. The analysis of our data indicates a more woody landscape and a higher water table
8 level, related to increased monsoonal rainfall during the African Humid period (AHP) between
9 9.5 and 5.5 cal kyr BP. High insolation and orbital changes account for a northward migration
10 of the African Rain Belt and a reinforced West Africa monsoon. The amount of forest fires was
11 low and most likely of natural occurrence, as human density was very low. A short dry event
12 interrupts the AHP and gives rise to a weakly grassy landscape at around 8.2 cal kyr BP. This
13 drought of centennial scale (400 years) occurring between 8.4 and 8 cal kyr BP is concomitant
14 with the general cooling observed in the Northern Hemisphere. After a period of transition, the
15 millennial-scale Late Holocene dry period begins at 4.8 cal kyr BP. The low water table level,
16 resulting from a decrease in precipitation, coincides with the appearance of a grassy savanna
17 landscape. Insolation decrease and reduced vegetation were likely driven by a southward
18 migration of the African Rain Belt and a weakening of the monsoon. During the late Holocene
19 the “Niayes” zone evolved into a phase of environmental stress often interrupted by Little
20 Humid Periods (LHP) of centennial scale (500 and 600 years) respectively between 4.4 and 3.9
21 and between 1.1 and 0.5 cal kyr BP. After 0.5 cal kyr BP the decrease in precipitation and the
22 increase in savanna fires, probably of anthropogenic origin, favor the landscape opening.

23 **Keywords:** Holocene, “Niayes”-Senegal, Carbon isotopes, Rock-Eval[®] thermal analysis,
24 Charcoals, Monsoon, Palaeoenvironment.

1 **1 Introduction**

2 From 1970 to 1990, the regions extending from the Sahel to the Gulf of Guinea suffered almost
3 from continuous drought (Dai et al., 2004; Bell and Lamb, 2006), with a tendency towards
4 rainfall resumption over the last three decades (Salack et al., 2011; Sagna et al., 2015; Vischel
5 et al., 2019). These dry and wet phases correspond respectively to a retreat and a greater
6 penetration of the monsoonal flux on the African continent (Nicholson, 2000; Fontaine et al.,
7 2012; Lafore et al., 2012). This rainfall deficit was one of the most intense climatic signals in
8 this region, with severe environmental and socio-economic consequences. It has dramatically
9 raised the question of the nature and intensity of future climate changes and of their threats to
10 socio-economic development and environmental resources. Climate models suggest that West
11 African countries are likely to experience higher temperatures, lower annual precipitation and
12 be more susceptible to a rise of sea-level (Serdeczny et al., 2016). However, climate projections
13 towards 2050, especially rainfall projections, are highly uncertain in many low-latitude regions
14 (Solomon et al., 2009). In order to better identify the impacts, vulnerabilities, and threats of the
15 ongoing climate change affecting this region and its inhabitants, a better knowledge of past
16 climate variability, past landscapes and adaptability of the people in this region would be of
17 help to design adaptation strategies. During the Early and Mid-Holocene, between ca 11 and 5
18 cal kyr BP, West Africa experienced stronger and more extended monsoons than today
19 (Niedermayer et al., 2010; Lézine et al., 2011). Changes in orbital forcing have been identified
20 as key factors in this intensification, resulting in vegetation changes and, consequently, a
21 decrease in dust flux off Sahara and West African Sahel (deMenocal et al., 2000; Pausata et al.,
22 2016; Messori et al., 2018), which reached minimum values around 6 cal kyr BP (Cockerton et
23 al., 2014). Palaeoecological and palaeolimnological analyses (i.e. pollen, diatoms) have shown
24 that during the African Humid Period (AHP) large tropical areas have experienced an increase
25 in rainfall, resulting in extensions of lakes, river systems and wetlands (Maley and Brenac,

1 1998; Lézine et al., 2011). Although some climate models and hydrological reconstructions
2 suggest a locally abrupt end to this period, (rapid rise in dust flux, large-scale vegetation density
3 decline, general lowering of lake levels at higher African latitudes; deMenocal et al. 2000;
4 Egerer et al., 2017), other studies indicate the termination of the AHP was rather characterized
5 by a gradual decline in moisture availability at lower latitudes (Shanahan et al., 2015; Dallmeyer
6 et al., 2020), and southern Ethiopia (Trauth et al., 2018).

7 A marine sediment core taken off the mouth of the Senegal River (15-16°N), revealed an
8 interruption of the AHP at around 4.2 cal kyr BP coeval to a weakening in the monsoonal
9 activity (Bouimetarhan et al., 2009). High carbon isotopic ratios ($\delta^{13}\text{C}$) obtained from organic
10 matter of a peat bog in the northern coastal zone of Senegal also suggest a short, high-intensity
11 aridity phase at around 4.5 cal kyr BP (Fall et al., 1998). This drought of global significance at
12 around 4 cal kyr BP is believed to be the cause of the first Central Africa humid tropical forests
13 crisis (Maley et al., 2017). This climatic transition is reported in the sub-Saharan and Sahelian
14 zone, between the Atlantic and Lake Chad (Lézine, 1989; Fall et al., 2010; Maley and Vernet
15 2015). Although the impact of climate on environmental changes is major during this period,
16 the role of humans likely becomes central from the Mid-Holocene onwards (7.2 cal kyr BP).
17 The increase in human population and the introduction of pastoralism are seen as decisive
18 factors in the irreversible reduction of Sahelian ecosystems (Fuller et al., 2011). Thus, it is
19 conceivable that humans were also catalysts in accelerating the devegetation in the Sahara at
20 the end of the AHP. Today, the role of humans and climate in landscape dynamics at the end of
21 the AHP remains to be assessed.

22 While the discussion mainly focused mainly on the West African monsoon variability and
23 human impact, very little attention has been given to the origin and role of fires on the West
24 Africa northern tropical ecosystems. Under these general dryer conditions, the introduction of
25 domestic economy with the settlement of farmer communities during the Late Holocene, can

1 also be considered as an important drivers of the fires at the southern limit of the Sahara
2 (Huyssecom et al., 2004). From 3 cal. kyr. BP fires, probably more anthropogenic than natural,
3 have played an active role in the opening of savannas in northern Burkina Faso (Ballouche and
4 Neumann, 1995) and the formation of the tropical savanna ecosystems in northern West African
5 (Dupont and Schefuß, 2018). In northwest Senegal, however, a sedimentary charcoal record
6 covering the entire Holocene has not yet been studied. Here, we propose a multi-proxy study
7 based on stable carbon isotopes and sedimentary charcoal analysis from a core taken in a peat
8 bog at the north coast of Senegal. We evaluate the changes in the C₃ and C₄ components
9 according to the climate and the fire regime respectively. We propose a hypothesis regarding
10 the relationship between climate, human activities, fire regime and vegetation in this part of the
11 Sahel.

12 **2 Regional Setting**

13 **2.1 Site Description and Geomorphology**

14 The “Niayes” region is a 2 to 8 km wide coastal strip of sand dunes with freshwater peat bogs
15 in inter-dune depressions, fed by water table and precipitation. It is located along the northern
16 coast of Senegal (West Africa; Fig. 1a) between 14° and 16° N and between 16° to 17° W,
17 extending across 200 km from Saint-Louis in the north to Dakar in the south (Fig. 1b).

18 The Quaternary sedimentary deposits (Fig. 2a) correspond to peat bogs and dune systems
19 chronologically organized from east to west by “Ogolian” (20 to 12 cal kyr BP) fixed red dunes
20 of NE-SW direction, “Tafolian” (4 to 2 cal kyr BP) semi-fixed yellow high dunes of NNW-
21 SSE direction (Michel, 1973). After 2 cal kyr BP, several hundred-meter-wide active white
22 coastal dunes of rather complex morphology settled at the proximity of the Senegal shoreline.
23 The peat bogs and freshwater ponds located in inter-dune aquatic depressions (Fig. 1c, Fig 2a)
24 developed at the end of the Pleistocene and early Holocene when wetter climate conditions
25 prevailed (Lézine and Chateauneuf, 1991).

1 **2.2 Climate**

2 The climate in “Niayes” region is controlled by the seasonal migration of the Intertropical
3 Convergence Zone (ITCZ; Fig. 1a). In boreal summer, the ITCZ is displaced northwards and
4 enables humid South-South-Western air masses (monsoon flux) to penetrate the region and
5 bring precipitation from July to September. The movement of the ITCZ to the southern
6 hemisphere in boreal winter corresponds to the dry season which extends from October to June.
7 The mean annual rainfall varies from 300 mm to 500 mm along a North-South gradient. Mean
8 annual temperature increases from 24.5°C on the coast to 26.3°C at the continental limit of the
9 “Niayes” (Aguiar et al., 2010).

10 **2.3 Vegetation**

11 Modern vegetation has been studied by different authors since 1940 (Adam, 1953; Fall et al.,
12 1998). The “Niayes” are hygrophilous vegetation enclaves surrounding littoral ponds and to
13 which the presence of the oil palm tree (*Elaeis guineensis*) gives a Guinean character. *Elaeis*
14 *guineensis* is characteristic of the area, but other less remarkable plant species are associated
15 with it (Adam, 1953). Flooded “Niayes” are characterized by a dominance of ferns. However,
16 wet and not flooded “Niayes” are invaded by woody vegetation and climbers. Around the
17 “Niayes” depressions, when the arboreal stratum decreases, grasses develop within the more or
18 less swampy waterlogged environment. *Typhaceae*, *Phragmites* and *Cyperaceae* that do not
19 have the same ecological requirements, show a different vegetal zonation and follow a spacial
20 distribution according to the soil moisture (Fig. 2b; Fall et al., 1998). Today, due to the lowering
21 of the water table or the non-filling of depressions, the area is turning into a steppe. The absence
22 or the disappearance of some species shows a regressive trend in natural flora, as compared to
23 the vegetation groups described by Trochain (Fall et al., 1998).

24 **2.4 Population**

1 Very little archeological studies have been conducted in the “Niayes” area. The decrease in
2 rainfall in the Sahara at the AHP termination is the cause of human dispersal including a
3 southward migration (Drake et al., 2011). This is particularly reflected in the increase in
4 settlements in the coastal Sahel between 7.5 and 6.5 cal kyr BP (Manning and Timpson 2014).
5 However, in the “Niayes”, traces of older human activities (hunting and farming) are described
6 by the presence of lithic materials (frames, blades and flint knives) dating from the Neolithic
7 (9.5 to 4.1 cal kyr BP). Humans used to settle on the dunes, because the inter-dune depressions
8 were frequently inundated. Cereal consumption was also indirectly evidenced by the presence
9 of wheel fragments and millet ear impressions on ceramics (Fare et al., 2017). Between the 13th
10 and 14th centuries AD, the ethnic group “Mandingue” temporarily occupied the zone. Around
11 1680 AD, a seasonal occupation by the “Wolof” ethnic group for farming (millet, peanut) and
12 Fula for pasture have been documented (Fuller et al., 2011).

13 **3 Material and Methods**

14 **3.1 Vegetation and Sediment Core Sampling**

15 Plant samples and a sediment core of 315 cm of long were collected in December 2015. 32
16 plant samples were taken along a North-South coastal transect (Saint-Louis to Saloum delta)
17 for C and N isotopic ratios and contents analyses. Plants were identified at the Botanical
18 Laboratory of Cheikh Anta Diop University (Senegal). They belong to 16 families and 20
19 species. Our plant sampling is characterized by an important number of *Poaceae* (six species)
20 and *Fabaceae* (four species) among the 20 species that have been randomly collected (Table
21 1). The sediment core was collected with a Russian corer in a peat bog located close to Mboro
22 village to 15°08'45''N and 16°53'18''W (Fig. 1c). The core was sampled each cm allowing for
23 fine-scale temporal resolution analysis.

24 **3.2 Radiocarbon Dating**

1 Radiocarbon age determinations were performed at Poznań Radiocarbon Laboratory on seven
2 samples of bulk sediment taken at depths of 15, 45, 95, 125, 155, 195 and 310 cm. All ^{14}C yr.
3 BP ages were converted into cal BP using the radiocarbon calibration program Calib 7.1 and
4 IntCal20 calibration curve (Reimer et al., 2020). An age-depth model was produced using R
5 version 3.5.0 of the software Bacon (Blaauw and Christen, 2011).

6 **3.3 Stable Carbon Isotopic Composition and C, N Contents**

7 65 samples were taken at 1, 3 and 6 cm depth and then each 5 cm along the core and measured
8 for carbon stable isotopic ratios ($\delta^{13}\text{C}$), and carbon (C) and nitrogen (N) contents of sedimentary
9 organic material. As no differences in carbon stable isotopic composition were observed on ten
10 of these samples, covering the different lithology layers of the core, with and without washing
11 pretreatments with 0.5 N hydrochloric acid (Nguetsop et al., 2011), we performed the isotopic
12 analyses of Mboro peat core on bulk sediment to derive past aboveground vegetation isotopic
13 signature. We also analysed 23 fresh plants sampled between December 2015 and January
14 2017. Rinsed plants and sediment samples were dried at 50°C overnight, ground using an agate
15 mortar and sieved through a $125\ \mu\text{m}$ mesh. Between 0.4 and 2 mg of sediment and plant powder
16 were weighed into tin capsules and analysed with an Isotopic Ratio Mass Spectrometer coupled
17 to an Elemental Analyser Pyrocube system at LEHNA (Lyon University). Results are expressed
18 as $\delta^{13}\text{C}$ using the conventional delta (δ) notation relative to the Vienna Pee Dee Belemnite (V-
19 PDB) for C isotopic ratios:

$$20 \quad \delta^{13}\text{C} (\text{‰}) = \left[\left(\frac{^{13}\text{C}/^{12}\text{C}_{\text{sample}}}{^{13}\text{C}/^{12}\text{C}_{\text{standard}}} \right) - 1 \right] \times 1000.$$

21 Analytical precision for $\delta^{13}\text{C}$ is better than 0.1 ‰. Results of elemental C and N contents are
22 expressed as (%) and are also presented as TC/TN ratios.

23 **3.4 Rock-Eval[®] (RE) Thermal Analysis**

1 Rock-Eval® thermal analysis of 10 samples each of about 100 mg (1, 20, 50, 100, 140, 180,
2 210, 250, 290 and 315 cm depth) along Mboro core was performed following the protocol
3 described by Sebag et al. (2013) with a Rock-Eval® 6 device manufactured by Vinci
4 Technologies. Standard parameters, namely Total Organic Carbon (TOC), Hydrogen Index
5 (HI), and Oxygen Index (OI), were calculated by integrating the amounts of hydrocarbon
6 compounds (HC, CO, and CO₂) produced during thermal cracking and combustion of the
7 organic matter. The correlation (HI vs OI) or the OI/HI ratio aims to characterize the origin and
8 decomposition of OM. Very high HI values and very low OI values (low OI/HI ratio) indicate
9 fresh aquatic or autochthonous organic matter origin while the increase in OI and the decrease
10 in HI (high OI/HI ratio) reflect an allochthonous source.

11 **3.5 Charcoal Analysis**

12 For macroscopic charcoal analyses, 0.5 cm³ samples taken from each cm slice were treated in
13 an aqueous 10 % KOH, 3 % (NaPO₃)₆ to facilitate de-flocculation and NaOCl solution to easily
14 separate the charcoals from bleached organic matter. Solutions were stirred overnight, sieved
15 at 160 µm, and washed with tap water. Charcoal particles were counted and their areas and
16 width/length ratios estimated under a binocular microscope equipped with a camera (CMEX-
17 5000) and connected to a computer with image analysis WinSeedle software. Only charcoals
18 with areas smaller than 0.2 mm² were used for analyses, the others were considered as outliers.
19 Total charcoal areas per unit volume of sediment (mm².cm⁻³) is a proxy for determining the
20 biomass burned and the frequency of fire occurrence. The width/length ratio (W/L) of charcoal
21 fragments was calculated to assess woody charcoal contribution versus grasses as described in
22 Alleman et al. (2013) assuming that elongated charcoal (W/L < 0.6) is preferentially produced
23 by grass fuel, while compact charcoal is preferentially produced by woody fuel (W/L > 0.6).

24 **4 Results**

1 **4.1 Core Description, Age-Model and Sedimentation Rate**

2 The analysis of the lithology and sedimentary structures of Mboro core along its 315-cm length
3 shows three units (Fig. 3b). The first unit (315-229 cm) is characterized by organic coarse sands
4 at the base of the core (315 to 302 cm) and silty sandy organic muds between 301 and 229 cm.
5 The second unit (228 and 94 cm) consists of black humic peat and the third one (93 and 3 cm)
6 of brown fibrous peat. The upper two centimeters of the core are composed of plant debris.
7 The calibrated ages of the seven conventional radiocarbon dates of Mboro core (Table 2, Fig.
8 3) cover the Holocene, between 9356 cal yr BP (310 cm) and 851 cal yr BP (15 cm).
9 Considering that the top of the core represents the modern period, an age-depth model (Fig. 3a)
10 can be considered, using six dates among the seven, assuming that the age determination at 45
11 cm is an outlier. The sedimentation rate is about 0.5 mm / year in the deeper part of the Mboro
12 core (310-120 cm). In the upper part of the core the age-depth model would suggest a lower
13 sedimentation rate after the Mid-Holocene (about 0.2 mm/year).

14 **4.2 Geochemistry**

15 **4.2.1 Modern Vegetation**

16 Leaf $\delta^{13}\text{C}$ values spanned from -32.1 ‰ to -13.2 ‰, covering the whole C_3 to C_4 plant isotopic
17 ranges (Fig. 4a, Table 1). The average $\delta^{13}\text{C}$ value for sampled C_3 plants is -28.3 ± 1.6 ‰, the
18 more depleted values (< -30 ‰) having been found in the *Arecaceae*, *Meliaceae*, *Lamiaceae*,
19 *Fabaceae* families (Table 1). The highest $\delta^{13}\text{C}$ values were found in the *Amaranthaceae* sample.
20 Most *Poaceae* species are C_4 plants, with an average $\delta^{13}\text{C}$ value of -14.3 ± 0.7 ‰. To compare
21 modern plants with those of the past, the increase of $\text{CO}_2\text{-atm}$ and the decrease of its $\delta^{13}\text{C}_{\text{CO}_2\text{-atm}}$
22 composition must be taken into account. Modern plants growing under about 400 ppmv
23 atmospheric pCO_2 and an averaged modern atmospheric CO_2 $\delta^{13}\text{C}$ of about -8.5 ‰ (Graven et
24 al., 2020), are depleted by about 1.6 ‰ compared to the Pre-Industrial era. Therefore, we
25 corrected $\delta^{13}\text{C}$ values of modern plant for this Suess effect (Fig. 4a; Suess, 1955; Nadelhoffer

1 and Fry, 1988). Most of C/N ratios ranged from about 12 to 33 except for 3 *Poaceae* samples
2 (43.9 to 96.8) and one *Cyperaceae* sample (45.8). The two families sampled in Mboro peat bog
3 showed more depleted $\delta^{13}\text{C}$ value and higher C/N ratios (Fig. 4a, Table 1) for the *Typhaceae* (-
4 27.7 ‰; 25.8), as compared to *Nympheaceae* (-24.3 ‰; 15.9).

5 **4.2.2 Mboro Core Isotopic Composition and TC, TN Contents**

6 The bulk organic carbon $\delta^{13}\text{C}$ values of the Mboro peat bog ranged between the C₃ and C₄ end-
7 members (Fig. 4b). Along depth, they display two major phases: below and above about 170
8 cm depth (Fig. 5a, Table 3). From the base to about 170 cm, $\delta^{13}\text{C}$, while fluctuating between -
9 22.2 ‰ (around 305 cm) and -27.6 ‰ (230 cm), exhibits a decreasing trend covering Unit 1
10 and the deepest part of Unit 2, with a slight but noticeable increase in $\delta^{13}\text{C}$ values at about 260
11 cm. The highest values are not the result of pedogenic carbonate as revealed by the similar
12 values of $\delta^{13}\text{C}$ in acid-washed samples, and the low inorganic carbon as shown by the Rock-
13 Eval® thermal analysis (Fig. 5a). The second phase, from 170 cm to the top of the core,
14 covering the upper part of Unit 2 and Unit 3, is characterized by a general increasing trend of
15 $\delta^{13}\text{C}$ (from about -26 to -18 ‰). This trend is not steady and consists of three $\delta^{13}\text{C}$ changes to
16 more positive values; around 140-100 cm (-22.7 ‰ to -17.4 ‰), 45 cm (-18.4 ‰), and near the
17 surface of the core (about -18.7 ‰), interrupted by two periods of lower $\delta^{13}\text{C}$, -24.6 ‰ and -
18 23.2 ‰ around 95 cm and 15cm, respectively. Positive shifts of $\delta^{13}\text{C}$ at 140 cm and 100 cm are
19 correlated with highest inorganic carbon contents. The pedogenic carbonate likely influenced
20 $\delta^{13}\text{C}$ at those specific depths.

21 The carbon, and nitrogen contents range between 2.8 and 53.3 %, and 0.2 and 2.3 %, respectively
22 (Table 3). Both TC and TN elements follow the same trend along the Mboro core.
23 The lowest values are recorded at the depth of 225 cm and three major peaks are observed at
24 165, between 100 and 90, and at 40 cm (Table 3). TC/TN ranges between 10 and 26 (Fig. 5b).
25 These ratios display small amplitude changes in the base of the core (about 13 to 18), while in

1 the upper part we observe much stronger variations and amplitude ranges (from 10 to 26) with
2 peak excursions at 150 cm, 100 cm and 50-40 cm ($TC/TN > 24$). The lowest TC/TN values are
3 observed in the upper part (20 cm to 0; Table 3, Fig. 5b). Acid-washed samples show similar
4 TC/TN ratios than untreated samples in the lower part of the core and slightly higher in the
5 upper part and substantially higher at 170 and 190 cm depth corresponding to the loss of the
6 more labile nitrogen during the acid washing process (Table 3).

7 **4.2.3 Rock-Eval® Thermal Analysis**

8 The selected samples of Mboro core are characterized by low OI values (96 to 205 mg O₂/g
9 TOC) and variable HI values which extend between 149 and 541 mg HC/g TOC (Fig. 6a, Table
10 3). Three sample groups can be distinguished through HI and OI diagram (Fig. 6b). The sample
11 at the bottom of Unit 1 (315 cm) is characterized by the highest HI value (541 mg HC/g TOC)
12 and the lowest OI value (96 mg O₂/g TOC). This sample belongs to group 2 (terrestrial material
13 origin). Samples from the upper part of Unit 2 (between 140 and 100 cm) characterized by low
14 HI and OI values, respectively ranging from 149 to 212 mg HC/g TOC and from 153 to 168
15 mg O₂/g TOC fall in group 3 (detrital material origin). The other seven samples are located
16 outside and between groups 1, 2, and 3. Two of these samples of the upper part of Unit 1,
17 between 290 to 250 cm, are closer to group 1 (Aquatic source) and characterized by HI and OI
18 of about 400 mg HC/g TOC and 100 mg O₂/g TOC respectively. OI/ HI ratio of the sample of
19 Unit 3 at 50 cm is within the range of those measured at 140 and 100 cm (group 3). Samples
20 located at 210 cm and 180 cm (lower part of Unit 2) and those at 20 cm and 1 cm (upper part
21 of Unit 3) lie between groups 1, 2, and 3, show HI values ranging from 295 to 350 mg HC/g
22 TOC and OI values, from 114 to 145 mg O₂/g TOC and similar OI/HI ratio (Fig. 6a, Table 3).
23 It is noteworthy that TC/TN and OI/HI ratios of Mboro sediments show a very good covariance
24 ($R^2 = 0.71$; Fig. 6a). TC/TN ratio covaries well with OI ($R^2 = 0.59$) and slightly less with HI
25 ($R^2 = 0.39$).

1 **4.3 Charcoals Total Area and Width/Length Ratio**

2 Charcoal concentration expressed in mm^2 per cm^3 along the Mboro core (Fig. 5d, Table 3) is
3 low from the base to about 100 cm with levels oscillating between 0 and $2.8 \text{ mm}^2 \cdot \text{cm}^{-3}$. Within
4 this phase, slight increases in charcoal concentration are registered between 260-240 cm and
5 170-120 cm. From 100 cm to the surface of the core, the background level is higher than in the
6 deeper section and high charcoal concentrations (from 2.2 to $15.6 \text{ mm}^2 \cdot \text{cm}^{-3}$; Table 3) are
7 registered at the depths of about 100, 86, 77, 54, 40-29 and 7 cm. The proportion of compact
8 charcoal ($\%W/L > 0.6$), predominantly originating from arboreal fuel, increases from the bottom
9 of the core to 200 cm depth (Fig. 5c). This trend is interrupted by a phase with lower proportions
10 of compact charcoal, between approximately 260 and 240 cm. From 200 to 34 cm, the
11 proportion of compact charcoal tends to decrease, reaching its lowest values (0.03). In this part
12 of the core, the first strong decrease from 200 to 133 cm is followed by a slight increase until
13 80 cm before decreasing again until 34 cm. The proportion of compact charcoal dramatically
14 increases from 35 to about 20 cm, and then shows a new decrease until the surface of the core.

15 **5 Discussion**

16 **5.1 Climatic and Environmental Interpretation of Bio-indicators and Geochemical** 17 **Proxies With Respect to Age Model**

18 The Mboro core in the “Niayes”, at the northern Atlantic coast of Senegal recorded significant
19 changes in environmental and climatic conditions during the Holocene, as also observed in
20 other tropical Northwest African environments (Lézine and Chateauneuf, 1991; deMenocal et
21 al. 2000; Lézine et al., 2011; Cockerton et al., 2014; Shanahan et al., 2015). To interpret the
22 sedimentary isotopic variations of the $\delta^{13}\text{C}$ (Fig. 5a), we relied on the principle of actualism, by
23 using geochemical features of modern vegetation of Senegal. Plants C/N values (all > 10 ; Table
24 1) enabled us to suggest that the organic matter deposited throughout the Mboro sequence has
25 a terrestrial origin ($10 < \text{TOC}/\text{TN} < 26$; Table 3). Moreover, Mboro C/N ratios suggest that the

1 site has always been filled with water during the Holocene, though higher TC/TN may be
2 indicative of periods with lower water tables and vice versa (Fig. 5b). Comparing the carbon
3 isotopic composition of sediment organic matter to that of modern plants indicates the
4 dominance of C₃ plants during the first half of the Holocene at Mboro site, more particularly
5 during the wettest period of the AHP (7.8 to 5.8 cal kyr BP). Organic matter $\delta^{13}\text{C}$ points towards
6 C₄ plants during the second half of the Holocene (Table 3, Fig. 7a). The terrestrial origin
7 attribution to organic matter from the TC/TN ratio also seems consistent with the OI/HI ratio
8 (Fig. 6a).

9 The data from Mboro evidenced two major phases of change on the northern coast of Senegal.
10 The first phase characterized by low $\delta^{13}\text{C}$, TC/TN and OI/HI values and low charcoal
11 concentration marks a humid period ranging from 9.4 to 5.5 cal kyr BP, interrupted by a short
12 arid phase around 8.2 cal kyr BP. The second phase, with irregular and often very high $\delta^{13}\text{C}$,
13 TC/TN and OI/HI values and higher charcoal concentration indicates a more arid major phase
14 from 4.8 cal kyr BP, interrupted by two Little Humid Periods (LHP).

15 **5.2 Early and Mid-Holocene (ca 9.4 to 5.5 cal kyr BP) Moist Climate : Tropical** 16 **Vegetation Development and Natural Forest Fires Weakness**

17 The Mboro fossil organic matter, of terrestrial origin (TC/TN >10; Fig. 5b), is marked by the
18 lowest values of $\delta^{13}\text{C}$ (-27.6 to -22.2 ‰; Fig. 5a, Fig. 7a) with a mean $\delta^{13}\text{C}$ value of -24.8 ± 1.4
19 ‰ attesting C₃-dominated vegetation. This is corroborated by the relatively high charcoal
20 particle W/L ratios suggesting wooded-dominated vegetation (Fig. 5c, Fig. 8a). The carbon
21 isotopes of organic matter show that during the Early and Mid-Holocene at the Mboro site the
22 proportion of C₃ plants increased to a maximum about 7.8 cal kyr BP. This increase was not
23 linear, and was interrupted, at about 8.2 cal kyr BP, by a period when C₃ plants either underwent
24 a strong water stress, resulting in increasing $\delta^{13}\text{C}$ due to stomata closure, or declined in favor
25 of C₄ plants. This is likely caused by climate change rather than by human activities, as indicated

1 by changes in precipitation, increased Monsoon dynamics, changes in thermohaline circulation
2 (Alley and Ágústadóttir, 2005), and influence of El Niño Southern Oscillation (ENSO) at this
3 period (Barber et al., 1999).

4 **5.2.1 The “8.2 kyr Event”**

5 The part of the AHP preserved in our core from 9 to 5 cal kyr BP is not stable. Between 8.4 and
6 8 cal kyr BP, when a significant decrease of the $\delta^{18}\text{O}$ values of the ice in North GRIP indicates
7 lower temperatures (Fig. 7c), the $\delta^{13}\text{C}$ of palaeovegetation surrounding the Mboro area
8 increases by about 2 ‰ (Fig. 7a). This can be explained by precipitation reduction or air
9 temperature decrease at 15°N (Fig. 7b). Concomitantly the charcoal concentration increases
10 and the W/L ratio decreases slightly (Fig. 8a-b), showing a slight fire regime increase and a
11 development of C₄ grasses and/or drought tolerant C₃ tree species, due to a short dry or cooler
12 episode during the AHP in the “Niayes” zone. Although this drought of centennial scale (400
13 years) is of smaller amplitude compared to other drought events recorded later in this Mboro
14 core, it is however significant (2 ‰) and is perfectly synchronous to North GRIP ice core $\delta^{18}\text{O}$
15 drop (Rohling and Pälike, 2005). Interestingly, the same pattern is observed in a nearby $\delta\text{D}_{\text{wax}}$
16 record off Senegal at 15°N (Niedermayer et al., 2010) and on the $\delta\text{D}_{\text{corr.}}$ of the Lake Bosumtwi
17 sediment core (Ghana) at 6°N (Fig 7d; Shanahan et al., 2015) despite the lower temporal
18 resolution of this core. In southern Sahara between 19°N and 23°N, the “8.2 kyr event” appears
19 to have lasted for a millennium or more as indicated by bioturbation forward modeling (Tierney
20 et al., 2017). These changes coeval the general cooling observed in the Northern Hemisphere
21 described in North Atlantic marine cores and Greenland ice cores (Fig. 7c; Rohling and Pälike,
22 2005). The Agassiz and Ojibway lakes massive freshwater discharges caused a significant
23 slowdown in thermohaline circulation and initiated the most abrupt and widespread cold event
24 to have occurred during the AHP (Barber et al., 1999). The impact of this climate event in the
25 North Atlantic may have led to changes in atmospheric circulation by reducing the West African

1 monsoon activity (Alley and Ágústsdóttir, 2005), which required ecophysiological adaptations
2 by plants in response to precipitation and/or atmospheric temperature decrease (Fig. 7b). This
3 response reflects in the Mboro record by a $\delta^{13}\text{C}$ increase (ie. stomata conductance reduction;
4 closure of stomata to limit plant evapotranspiration). Cheng et al. (2009) have hypothesized that
5 the ITCZ, which brings precipitation to the tropics, shifted further south during the "8.2 kyr
6 event" in Central America. In North Africa, the tropical trees disappeared at the beginning of
7 this cooling event and the grasses underwent slight increase (Li et al., 2019). Through this high
8 temporal resolution study of the Mboro core, we suggest that the "8.2 kyr event" is synchronous
9 between high and low latitudes of the northern hemispheric and is reflected on the Northern
10 Coast of Senegal by a weakening of the monsoon of West Africa as in Asia. This phasing
11 between the north coast of Senegal and Greenland suggests the existence of an atmospheric
12 teleconnection (Liu et al., 2013).

13 **5.2.2 Active Monsoon System**

14 After 8 cal kyr BP, the resumption of the $\delta^{13}\text{C}$ decrease (Fig. 7a) suggests the return of a rainy
15 regime linked to a very active monsoon system. Proportion of C_3 plants in the vegetative cover
16 computed from $\delta^{13}\text{C}$ shows that it exceeded 90 % of at 7.6 cal kyr BP and between 6.9 and 6.4
17 cal kyr BP. The low charcoal concentration, the relatively high proportion of charcoal from
18 woody fuel (Fig. 8a-b) and the low human density at 15-16°N between 8 and 7 cal kyr BP (Fig.
19 8e1 and e2, Manning and Timpson, 2014) together points to a fire regime of rare or weak natural
20 forest fires, caused more likely by lightning in a wet environment (Tutin et al., 1996). High HI
21 values ($> 200 \text{ mg HC/g TOC}$) correlated with very low IO values ($< 200 \text{ mg O}_2/\text{g TOC}$; Fig.
22 7b) are compatible with high autochthonous organic matter inputs (Sebag et al., 2013) in the
23 deposit of the first peat levels around 7.5 cal kyr. BP (Fig. 3b). Heavy rainstorms (Maley, 1982)
24 may have caused the Upper Pleistocene dunes erosion, sand input and deposit in the inter-dune
25 depressions (Fig. 2a). The $\delta^{13}\text{C}$ values about -24 to -25 ‰ and TC/TN about 14-15 are consistent

1 with measured values on current *Nymphaeacea* (Table 1) and pollen study showing abundant
2 aquatic plants (*Nymphaea lotus*, *Potamogeton*, *Polygonum senegalense*) and higher water table
3 level (Lézine, 1989).

4 Thus, studies conducted at higher latitudes (20°N), off Cap Blanc (Northern Mauritania)
5 indicate low dust supply (Fig. 7e; deMenocal et al., 2000). The development of a forest-savanna
6 mosaic with predominantly C₃ plants in the vegetation and a high fire regime recorded between
7 10 and 6 cal kyr BP (Fig. 8c; Dupont and Schefuß 2018) would likely be related to human
8 presence in the Sahara during this period as shown by Manning and Timpson (2014). Fall et al.
9 (1998) indicate a more marked decrease of vegetation $\delta^{13}\text{C}$ around 6.2 cal kyr BP at 15°N, in
10 other “Niayes” peat bog (Touba Ndiaye) north of Mboro (Fig. 7f). This is synchronous with a
11 northward displacement of tropical vegetation of approximately 6 to 9°N compared to the
12 current position (Hély et al., 2014; Pausata et al., 2016). These results are in agreement with the
13 monsoon intensification from Western Sahara to the northwest of the Sahel between 10 and 6
14 cal kyr BP. The influence of ENSO (Barber et al., 1999), the orbital forcing changes that control
15 vegetation changes and the dust emissions from the Sahara have been identified as key factors
16 of the northward migration of the African Rain Belt and the precipitation intensification during
17 the AHP (Messori et al., 2018). We observed a precipitation synchronicity between the north
18 coast of Senegal and the coast of Morocco. However, the Green Sahara climate model shows
19 that the northern zone humidity was reinforced by two components: Mediterranean winter
20 precipitation and summer monsoon precipitation (Fig. 7g; Cheddadi et al., 2021).

21 On the northern coast of Senegal, the end of the wettest phase was abrupt (300 years) and
22 characterized by a C₃ vegetation decrease due to monsoon weakening between 5.8 cal kyr BP
23 and 5.5 cal kyr BP as suggested by the increase trend of $\delta^{13}\text{C}$ which will peak at 4.5 cal kyr BP
24 (-17.4‰; Fig. 7a). At the same time, the W/L ratio decrease suggests an increase in charcoal

1 composed of grasses (Fig. 8a). However, we observed that between 6.5 and 5.8 cal kyr BP, the
2 $\delta^{13}\text{C}$ varies almost in phase with the small climatic oscillations observed on the NGRIP ice core
3 (Fig. 7b; Rohling and Pälike, 2005). This is in agreement with other palaeo-records (Fig. 7e;
4 deMenocal et al., 2000) and climate models (Tierney et al., 2017) in North-West Africa showing
5 earlier wet phase and the abrupt end of the AHP (occurring within a few hundred years) around
6 5.5 cal kyr BP in Western Sahara and around 4.6 cal kyr BP at the northern Atlantic coast of
7 the Sahel region (Fig. 7f; Fall et al., 1998). However, in other records from more tropical sites
8 in Ghana (Lake Bosumtwi, Fig. 7d); Shanahan et al. (2015) recorded a time-transgressive
9 termination of the AHP. Northern-Cameroon (Lake Mbalang, Fig. 7h; Nguetsop et al., 2011),
10 Western-Cameroon (Lake Barombi Mbo, Maley and Brenac, 1998) and southern Ethiopia
11 (Trauth et al., 2018), showed the gradual extension of the wet phase until ca 3 cal kyr BP. This
12 variability between high and low latitudes is related to the fact that in the lower latitudes of
13 West Africa, where the rainfall is only influenced by the summer monsoon dynamics, the end
14 of the AHP coincides with the gradual retreat of the monsoonal rainfall belt (Dallmeyer et al.,
15 2020).

16 **5.3 Late Holocene Climate Oscillation (After 5 cal kyr BP)**

17 Climate change during the Late Holocene in sub-Saharan Africa has generated much debate in
18 recent decades. The West African monsoon variability has been the subject of controversy
19 depending on the proxy used and the location of the records. On the North coast of Senegal, our
20 study reveals complex climatic fluctuations characterized by two long dry phases of centennial
21 and millennium scale respectively from 4.8 cal kyr BP interrupted by two LHP of centennial
22 scale (500 and 600 years) between ca 4.4 and 3.9 and between ca 1.1 and 0.5 cal kyr BP
23 respectively. Our results agree with those of Fall et al. (2010) which described two dry phases
24 separated by two wet phases in another core from peat bogs near Mboro (Fig. 7i). In the alluvial
25 zone of the Senegal River mouth, Bouimetarhan et al. (2009) identified two long dry phases (ca

1 4.2 to 2.9 cal kyr BP and ca 2.5 to 1.5 cal kyr BP), each interrupted by a small wet phase; the
2 first between 2.9 and 2.5 cal kyr BP and the other between 1.5 and 1.2 cal kyr BP. However,
3 these results are opposed to other palaeoecological records which, for the most part, have shown
4 two dry phases (the first between 4.5 and 4 cal kyr BP and the other after 2 cal kyr BP) separated
5 by a long wet phase (ca 4 to 2 cal kyr BP) in the Northwest of the Sahel (Lézine, 1989; Lézine
6 and Chateauneuf, 1991).

7 **5.3.1 The Dry Phases**

8 *i. The 4.5 Kyr BP Drought: Tropical Vegetation Collapse and the Onset of* 9 *Anthropogenic Fires*

10 From 4.8 cal kyr BP, $\delta^{13}\text{C}$ values (Fig. 7a), TOC/TN and OI/HI ratios (Fig. 6a) increase and
11 reach respective maxima of -17.7 ‰, 25.6, and 1.12 around 4.5 cal kyr BP. This suggests an
12 increase of allochthonous organic matter input from a detrital source and the development of
13 C_4 plants, mainly *Poaceae*, around the bog, as shown by the high TOC/TN values of modern
14 C_4 plants (Table 1). $\delta^{13}\text{C}$ values and TOC/TN then rapidly decrease to reach their pre-4.8 cal
15 kyr BP values. These peaks are consistent with the occurrence of a major arid event,
16 characterized by the lowering of the water table in the inter-dunes, and the tropical vegetation
17 collapse. This event is very rapid, with the phase of aridification lasting about 300 years, while
18 it ends even more quickly, in less than 100 years. A slight increase in fire occurrence is indicated
19 by an increase in sedimentary charcoal, dominated by grass charcoal fragments (Fig. 8a-b).
20 During this period the fire regime decreases at 20°N (Fig. 8c; Dupont and Schefuß, 2018),
21 possibly caused by the rarefaction of vegetation fuel and human retraction in Central Sahara, in
22 relation with the end of the AHP. Concomitantly, there is evidence of an increase in human
23 occupation on the north coast of Senegal (Fig. 8e3), of significant demographic development
24 on the southwest coast of Sahara (Fig. 8d; Manning and Timpson 2014). This is consistent with
25 the presence of different groups of humans in the “Niayes” during the final Neolithic between

1 ca 5 and 4 cal kyr BP (Fare et al., 2017). The increased fire regime evidenced at Mboro during
2 this period is then certainly related to this human demographic change.
3 These results support the hypothesis of an abrupt drought, less than 400 year-long which marks
4 the Late Holocene onset. This centennial-scale event was evidenced throughout Sub-Saharan
5 Africa, with a variable temporal extent depending on the location. On the north coast of Senegal,
6 the Touba Ndiaye palaeorecord, in a Niayes peat bog north of Mboro, evidenced the
7 development of *Cyperaceae* and C₄ plants (Fig. 7f; Fall et al., 1998). The gradual disappearance
8 of the mesophilic forest association with Guinean species started around 7.5 cal kyr BP
9 continued until 4.5 cal kyr BP (Lézine, 1989). This period coincides with the African monsoon
10 weakening from the tropical north Atlantic coasts between 15° and 16°N and the onset of
11 “Niayes” opening. Further north, off the Senegal River mouth, the GeoB9503 marine core data
12 indicate by the considerable Sahelian savanna pollen representation (*Poaceae* and *Cyperaceae*)
13 and the presence of semi-desert species, such as the *Asteroidae*, relatively dry conditions with
14 a longer duration of about 1300 years, between about 4.2 and 2.9 cal Kyr BP (Bouimetarhan et
15 al., 2009). In Cap Blanc, the dust flux increases rapidly and reaches a maximum and then
16 remained constant throughout the Late Holocene (Fig. 7e; deMenocal et al., 2000). In the
17 Guinea Gulf, this “4.5 kyr event” coeval the rainforests fragmentation (Maley et al., 2017) and
18 the Dahomey gap opening between ca 4.8 and 3.4 cal kyr BP (Fig. 7j; Salzmann and
19 Hoelzmann, 2005). In Lake Mbalang (Northern Cameroon), this event is characterized by a
20 small increase of the $\delta^{13}\text{C}$ suggesting slight dryer conditions (Fig. 7h; Nguetsop *et al.*, 2011)
21 while it is not noticeable at Lake Barombi Mbo (South Cameroon, Maley and Brenac, 1998).

22 **ii. Grass Savanna Development and Anthropogenic Fires Intensification (ca 2.8 to 1.3**
23 **cal kyr BP)**

24 A longer period, but less arid than the 4.5 cal kyr arid event, occurs between ca 2.8 and 1.3 cal
25 kyr BP. From 2.8 to ca. 2.3-2.1 cal kyr BP, $\delta^{13}\text{C}$ and TOC/TN values increase and reach maxima

1 of -18.4 ‰, and 25.6 respectively, while OI/HI ratios remain high (Fig. 7a, Fig. 6a). These
2 values indicate another water table level decrease in the inter-dunes, C₄ plants development and
3 allochthonous source of organic matter probably dominated by *Poaceae*. Savanna, dominated
4 by herbaceous plants as shown by W/L ratio was subject to more intense fires than in the
5 previous dry period (Fig. 8a). This fires intensification is to be related to the settlement of a
6 dense human population on the North coast of Senegal (15°N) around 3 cal kyr BP (Fig. 8e4;
7 Manning and Timpson, 2014) corresponding to the onset of the Iron Age (Fare et al., 2017).
8 “Niayes” gradually became a hunting and agricultural area, likely prone to regular
9 anthropogenic fires keeping vegetation in an open savanna state where herbaceous consists
10 mainly of C₄ grasses (Bond and Keeley, 2005). This is consistent with a study in northern
11 Burkina Faso, where archaeological charcoal illustrates the development of the West African
12 savanna as a cultural landscape at the end of this period (Höhn and Neumann, 2012). This arid
13 period coeval with the high percentage of Saharan (*Asteroidae*) and Sahelian (*Acacia*,
14 *Mimosa*) species found off the Senegal River mouth (Bouimetarhan et al., 2009). Our
15 reconstructions show a dry period of about 1500 years while Fall et al (2010) estimated a dry
16 period of 1000 years, between 2.5 and 1.5 cal kyr BP (Fig. 7i) due to reduced monsoonal
17 rainfalls in the Sahelian latitudes (Lézine, 1989; Maley et al., 2017).

18 **5.3.2 The Wet Phases**

19 *i. The Late Holocene « First Little Humid Period (FLHP) » (ca 4.4 to 3.9 cal kyr BP)*

20 The strong decrease in $\delta^{13}\text{C}$ values (Fig. 7a), and the slight decrease in TOC/TN and OI/HI
21 ratios (Fig. 6a) between ca 4.4 and 3.9 cal kyr BP indicate an increase in the amount of C₃
22 plants, a detrital material input (Fig. 6a-b) and consequently a first Little Humid Period (FLHP)
23 interrupting the Late Holocene drought. Despite the human density increased in the north-west
24 of Senegal (Fig. 8e3; Manning and Timpson 2014; Fare et al., 2017), the humid climate caused
25 a decrease in fires and a slight increase in charcoal fragments from woody vegetation as shown

1 in the W/L ratio (Fig. 8a). This Late Holocene FLHP ended with an intense return of fire
2 regimes without a change in fuel type (constant W/L) between 4.1 and 3.8 cal kyr BP. The high
3 charcoals peak probably suggests that the fire frequencies and intensities are not related to the
4 aridity degree but to the availability and abundance of the biomass to be burned (Aleman et al.,
5 2013).

6 This Late Holocene FLHP, occurring after the dry event marking the termination of the AHP is
7 well described in records in the north-western Sahel, but at different ages and time extents. In
8 the Senegal “Niayes” zone, it was described by Fall et al. (2010) around 3 cal kyr BP (Fig. 7i).
9 The development of Guinean species around 3.5 cal kyr BP (Lézine, 1989) reflected more
10 pronounced local humid conditions and a rise in water table level. Off the Senegal River mouth,
11 Bouimetarhan et al. (2009) recorded a strong and rapid moisture increase between ca 2.9 and
12 2.5 cal kyr BP. Further north in Cap Blanc (Mauritania), Dupont and Schefuß (2018) evidenced
13 it between 3.5 and 3 cal kyr BP. It is correlated with wetter conditions that have been described
14 in marine sediments off the West African coast (Einsele et al., 1974). In the rainforest belt, this
15 period was longer. A period with high lake water levels was evidenced between 2.5 and 1.5 cal
16 kyr BP in Lake Bosumtwi in Ghana (Talbot and Delibrias, 1980; Shanahan et al., 2009;
17 Shanahan et al., 2015; Fig. 7d) and between 3.3 and 1.1 cal kyr BP in Lake Sélé in Benin (Fig.
18 7j; Salzmann and Hoelzmann, 2005). The precipitation rate increase may have been caused by
19 the northward migration of the tropical rainfall zone and by the maximum intensification of
20 monsoon rain over Sahelian latitudes as suggested by astronomical models (Short and Mengel,
21 1986).

22 **ii. *The Late Holocene « Last Little Humid Period (LLHP) » (ca 1.1 to 0.5 cal kyr BP)***

23 The decrease in $\delta^{13}\text{C}$, TOC/TN and OI/HI ratios between ca 1.1 and 0.5 cal kyr BP, indicates a
24 second LHP but of lesser intensity than that of the onset of the Late Holocene (Fig. 6a; Fig. 4b).

1 It is marked by a maximum development of C₃ plants (Fig. 7a) and an organic matter input of
2 aquatic origin (Fig. 6b) at ca 0.85 cal kyr BP. Despite increasing human occupation, the fire
3 regime weakened and the proportion of charcoal from woody fuel increased (Fig. 8a), which
4 confirms the humidity in the area around 1 cal kyr. BP. The Mboro high-resolution record
5 results and other $\delta^{13}\text{C}$ (Fig. 7i; Fall et al., 2010), pollen and diatom records (Lézine et al., 2019)
6 in the “Niayes” area and further north off Senegal (Bouimetarhan et al., 2009) picture a short
7 stabilization of tropical plant contents, due to a return of some monsoonal rainfall at the onset
8 of the last millennium. This several-century-long wet period can be considered as the Late
9 Holocene LLHP. However, it has not been clearly evidenced by proxies in other sub-Saharan
10 Africa sites.

11 **5.3.3 Towards the present Sahel: grassland development and fires reactivation since ca** 12 **0.5 cal kyr BP**

13 Two samples in our data could potentially represent a change in terrestrial vegetation over the
14 last five centuries, evidenced by a TOC/TN ratio greater than 10 (Table 3, Fig. 6a). The
15 significant increase in $\delta^{13}\text{C}$ (-18.7 ‰; Fig. 7a) might indicate the installation of current Sahelian
16 conditions in the NW of subtropical Africa, concomitant with a strong human influx to the
17 “Niayes” depressions in search of agro-pastoral areas (Fare et al., 2017) and with land-use
18 changes. Fire regime reactivated, with fuel dominated by grasses (Fig. 8a-b). Their frequencies
19 gradually accelerated the vegetation degradation and contributed to the installation of the
20 current grassland environment under these latitudes (Dupont and Schefuß, 2018). Our results
21 agree with more detailed studies focusing on the last millennium, that indicate an increased
22 drought corresponding to the Little Ice Age (LIA, 1400-1850 EC) from 0.5 cal kyr BP in the
23 Baobab depression, “Niayes”-Senegal (Lézine et al., 2019) and at Lake Bosumtwi, Ghana (Fig.
24 7d; Shanahan et al., 2009; Shanahan et al., 2015). During this period, the Sahelian vegetation
25 seems to primarily respond to anthropogenic action (Fuller et al., 2011), which may mask the

1 influence of climate change (Ballouche and Neumann, 1995) and especially the effects of
2 monsoonal rainfalls variability.

3 **6 Conclusions**

4 The sediment core record from Niayes peat bogs in northwestern Senegal revealed local West
5 African climate variability over the past 10,000 years. The multiproxy approach used in this
6 study, which exceptionally covers almost the entire Holocene period, shows that both climatic
7 and anthropogenic forcings are involved in the vegetation evolution. The stable carbon isotope
8 geochemical analysis showed that during the AHP (9.5-5.5 cal kyr BP) climate was the main
9 factor influencing the vegetation which consisted mainly of C₃ plants. Forest fires were likely
10 natural, weak, and triggered by lightning in a wet environment where human density was very
11 low. A short arid episode of centennial scale (400-year-long) occurred between 8.4 and 8 cal
12 kyr BP. This “8.2 kyr event” is evidenced by slight increases of herbaceous plants and fire
13 regime during the mid-AHP.

14 At the end of the AHP, the depopulation of the central Sahara and the human migration to the
15 coastline and areas south of the Sahara begins to mitigate the climate influence on the Sahel
16 landscapes evolution. The onset of the Late Holocene (ca 4.5 cal kyr BP) is marked by a dry
17 period of centennial and millennium scale at the North coast of Senegal that has led to the
18 collapse of wooded vegetation. Increased human density in the “Niayes” initiated
19 anthropogenic fires of herbaceous savannas. The Late Holocene was not uniformly arid, being
20 interrupted by two LHP. The first was between ca 4.4 and 3.9 cal kyr BP and the last between
21 ca 1.1 and 0.5 cal kyr BP. These were marked by the resettlement of trees in the “Niayes”
22 depressions. The collapse of the woody vegetation coincided with the arid major phases, where
23 regular disturbance by anthropogenic fires likely promoted the open character of the vegetation.
24 During the Late Holocene anthropogenic action has progressively taken over from climate as a
25 primary determinant of vegetation composition.

1 **Acknowledgements.** We thank the Department of Geology-UCAD for conducting the field
2 works and the students Omar Baldé and Ibrahima Diouf for their participation. We are
3 particularly grateful to ISEM (Institut des Sciences de l'Evolution de Montpellier) provided
4 grant and fees for isotopic analyses. Special thanks also to Thierry Adate (Institute of Earth
5 Sciences, University of Lausanne, Switzerland) for his technical and scientific supports in
6 Rock-Eval[®] thermal analysis, a trademark registered by IFP Energies Nouvelles. Thanks are
7 due to CEFREM-Perpignan for the sedimentological analysis. We deeply acknowledge the
8 reviewers Dr C. Thompson and Dr Andrew Johnston for the English language revision.

9
10
11
12
13
14
15
16
17
18
19
20
21
22
23
24
25

1 **References**

- 2 Adam, J.G., 1953. Note sur la végétation des Niayes de la Presqu'Île du Cap Vert. Bull. Soc.
3 Bot. France, 100, 153–158.
- 4
- 5 Aguiar, L.A.A., Gameau, M., Lézine, A.M., Maugis, P., 2010. Évolution de la nappe des sables
6 quaternaires dans la région des Niayes du Sénégal (1958-1994): relation avec le climat
7 et les impacts anthropiques. Sécheresse, 21, 97–104.
- 8
- 9 Aleman, J.C., Blarquez, O., Bentaleb, I., Bonté, P., Brossier, B., Carcaillet, C., Gond, V.,
10 Gourlet-Fleury, S., Kpolitia, A., Lefèvre, I., Oslisly, R., Power, M.J., Yongo, O.,
11 Bremond, L., Favier, C., 2013. Tracking land-cover changes with sedimentary charcoal
12 in the Afrotropics. Holocene, 23, 1853 –1862.
- 13
- 14 Alley, R.B., Ágústadóttir, A.M., 2005. The 8k event: cause and consequences of a major
15 Holocene abrupt climate change. Quat. Sci. Rev., 24, 1123–1149.
- 16
- 17 Ballouche, A., Neumann, K., 1995. A new contribution to the Holocene vegetation history of
18 the West African Sahel: pollen from Oursi, Burkina Faso and charcoal from three sites
19 in northeast Nigeria. Veget. Hist. Archaeobot., 4, 31–39.
- 20
- 21 Barber, D.C., Dyke, A., Hillaire-Marcel, C., Jennings, A.E., Andrews, J.T., Kerwin, M.W.,
22 Bilodeau, G., McNeely, R., Southon, J., Morehead, M. D., Gagnon, J. M., 1999. Forcing
23 of the cold event of 8.200 years ago by catastrophic drainage of Laurentide lakes. Nature,
24 400, 344–348.
- 25

- 1 Blaauw, M., Christen, J. A., 2011. Flexible paleoclimate age - depth models using an
2 autoregressive gamma process. *Bayesian Analysis*, 6, 457–474.
3
- 4 Bell, M.A., Lamb, P.J., 2006. Integration of weather system variability to multidecadal regional
5 climate change: the West African Sudan–Sahel Zone. *J. Climatol.*, 19, 5343– 5365.
6
- 7 Bond, W. J., Keeley, J. E., 2005. Fire as a global “herbivore”: the ecology and evolution of
8 flammable ecosystems. *Trends, Ecol. Evol.* 20, 387–394.
9
- 10 Bouimetarhan, I., Dupont, L., Schefuß, E., Mollenhauera, G., Mulitza, S., Zonneveld, K., 2009.
11 Palynological evidence for climatic and oceanic variability off NW Africa during the
12 late Holocene. *Quat. Res.*, 72, 188–197.
13
- 14 Cheddadi R., Carré M., Nourelbait M., François L., Rhoujjati A., Manay R., Ochoa D., Schefuß
15 E., 2021. Early Holocene greening of the Sahara requires Mediterranean winter rainfall.
16 *PNAS* 118 (23), 1–7.
17
- 18 Cheng. H., Fleitmann. L., Edwards. D.R., Wang. X., Cruz. F.W., Auler. A. S., Mangini. A.,
19 Wang. Y., Kong. X., Burns. S. J., Matter. A., 2009. Timing and structure of the 8.2 kyr
20 B.P. event inferred from $\delta^{18}\text{O}$ records of stalagmites from China, Oman, and Brazil.
21 *Geology*, 37, 1007–1010, Doi: 10.1130/G30126A.
22
- 23 Cockerton, H.E., Holmes, J.A., Street-Perrott, F.A., Ficken K.J., 2014. Holocene dust records
24 from the West African Sahel and their implications for changes in climate and land
25 surface conditions. *J. of Geo. Res.: Atm.*, 14, 8684–8694.

- 1
- 2 Dai, A., Lamb, P.J., Trenberth, K.E., Hulme, M., Jones, P.D., Xie, P., 2004. Comment the recent
3 Sahel drought is real. *Int. J. Climatol.*, 24, 1323–1331.
- 4
- 5 Dallmeyer, A., Claussen, M., Lorenz, S.J., Shanahan, T., 2020. The end of the African humid
6 period as seen by a transient comprehensive Earth system model simulation of the last
7 8000 years. *Clim. Past*, 16, 117–140.
- 8
- 9 deMenocal, P., Ortiz, J., Guilderson, T., Adkins, J., Sarnthein, M., Baker, L., Yarusinsky, M.,
10 2000. Abrupt onset and termination of the African Humid Period: rapid climate
11 responses to gradual insolation forcing. *Quat. Sci. Rev.*, 19, 347–361.
- 12
- 13 Drake, N.A., Blench, R.M., Armitage, S.J., Bristow, C.S., White, K.H., 2011. Ancient
14 watercourses and biogeography of the Sahara explain the peopling of the desert. *PNAS*,
15 108, 458–462.
- 16
- 17 Dupont, L.M., Schefuß, E., 2018. The roles of fire in Holocene ecosystem changes of West
18 Africa. *Earth Planet. Sci. Lett.*, 481, 257–266.
- 19
- 20 Egerer, S., Claussen, M., Reick, C., Stanelle, T., 2017. Could gradual changes in Holocene
21 landscape have caused the observed abrupt shift in North Atlantic dust deposition? *Earth
22 Planet. Sci. Lett.*, 473, 104–112.
- 23
- 24 Einsele, G., Herm, D., Schwarz, H.U., 1974. Sea Level Fluctuation during the Past 6000 yr at
25 the Coast of Mauritania. *Quaternary Res.*, 4, 282–289.

- 1
- 2 Fall, M., Trimborn, P., Férhi, A., 1998. A $\delta^{13}\text{C}$ record of late Quaternary climate change in a
3 Senegalese peat bog. *Paleoecology of Africa*, 35, 21–28.
- 4
- 5 Fall, M., Gaye, J.P., Trimborn, P., 2010. Isotope refinement of late Holocene climatic
6 oscillations in the northern coast of Senegal. *Global Planet. Change*, 72, 331–333.
- 7
- 8 Fare, Y., Dufumier, M., Loloum, M., Miss, F., Pouye, A., Khastalani, A., Fall, A., 2017.
9 Analysis and Diagnosis of the Agrarian System in the Niayes Region, Northwest
10 Senegal (West Africa). *Agriculture*, 7, 59; 1–25. DOI: 10.3390/agriculture7070059.
- 11
- 12 Fontaine, B., Roucou, P., Camara, M., Vigaud, N., Konaré, A., Sanda, S.I., Diedhiou, A., and
13 Janicot, S., 2012. Variabilité pluviométrique, changement climatique et régionalisation
14 en région de mousson africaine. *Météorologie-Spécial AMMA.*, 41–48.
- 15
- 16 Fuller, D.Q., van Etten, J., Manning, K., Castillo, C., Kingwell-Banham, E., Weisskopf, A.,
17 Qin, L., Sato, Y-I., Hijmans, R.J., 2011. The contribution of rice agriculture and
18 livestock pastoralism to prehistoric methane levels: an archaeological assessment.
19 *Holocene* 21, 743–759. DOI: 10.1177/0959683611398052.
- 20
- 21 Gasse, F., 2000. Hydrological changes in the African tropics since the Last Glacial Maximum.
22 *Quat. Sci. Rev.*, 19, 189–211.
- 23

- 1 Graven, H., Keeling, R.F., Rogelj, J., 2020. Changes to carbon isotopes in atmospheric CO₂
2 over the industrial era and into the future. *Global Biogeochemical Cycles*, 34,
3 2019GB006170. [https://doi.org/ 10.1029/2019GB006170](https://doi.org/10.1029/2019GB006170).
- 4
- 5 Hély, C., Lézine, A.M., APD contributors, 2014. Holocene changes in African vegetation:
6 tradeoff between climate and water availability. *Clim. Past*, 10, 681–686.
- 7
- 8 Höhn, A., Neumann, K., 2012. Shifting cultivation and the development of a cultural landscape
9 during the Iron Age (0-1500 AD) in the northern Sahel of Burkina Faso, West Africa:
10 Insights from archaeological charcoal. *Quat. Int.*, 249, 72–83.
- 11
- 12 Huysecom, E., Ozainne, S., Raeli, F., Ballouche, A., Rasse, M., Stokes, S., 2004. Ounjougou
13 (Mali): a history of Holocene settlement at the southern edge of the Sahara. *Antiquity*,
14 78, 579–593.
- 15
- 16 Lafore, J.P., Asencio, N., Bouniol, D., Couvreur, F., Flamant, C., Guichard, F., Hall, N.,
17 Janicot, S., Kocha, C., Lavaysse, C., Leroux, S., Poan, E., Peyrillé, P., Roca, R., Roehrig,
18 R., Roux, F., Saïd, F., 2012. Évolution de notre compréhension du système de mousson
19 ouest-africain. *Météorologie-Spécial AMMA.*, 11–16.
- 20
- 21 Laskar, J., Robutel, P., Joutel, F., Gastineau, M., Correia, A.C. M., Levrard, B., 2004. A long
22 term numerical solution for the insolation quantities of the Earth. *Astron. Astrophys.*
23 428, 261–285.
- 24
- 25 Lézine, A.M., 1989. Late Quaternary Vegetation and Climate of the Sahel. *Quat. Res.*, 32,

1 317–334.

2

3 Lézine, A.M., Châteauneuf, J.J., 1991. Peat in the "Niayes" of Senegal: depositional
4 environment and Holocene evolution. *J. Afr. Earth Sci.*, 12, 171–179.

5

6 Lézine, A.M., Hély C., Grenier C., Braconnot P., Krinner G., 2011. Sahara and Sahel
7 vulnerability to climate changes, lessons from Holocene hydrological data. *Quat. Sci.*
8 *Rev.*, 30, 3001–3012.

9

10 Lézine, A.M., Lemonnier, K., Fofana, C.A.K., 2019. Sahel environmental variability during the
11 last millennium: Insight from a pollen, charcoal and algae record from the Niayes area,
12 Senegal. *Rev. Palaeobot. Palynol*, 271, 1–7.

13

14 Li, H., Renssen. H., Roche. D.M. Miller. P.A., 2019. Modelling the vegetation response to the
15 8.2 ka BP cooling event in Europe and Northern Africa. *J. Quaternary Sci.*, 1–12.

16

17 Liu, Y., Henderson, G., Hu, C., Mason, A., Charnley, N., Johnson, K., Xie, S., 2013. Links
18 between the East Asian monsoon and North Atlantic climate during the 8.200 years
19 event. *Nature Geos*, 6, 117–120.

20

21 Maley J., 1982. Dust, Clouds, Rain Types, and climatic variations in Tropical North Africa.
22 *Quat. Res.*, 18, 1–16.

23

- 1 Maley, J., Brenac, P., 1998. Vegetation dynamics, palaeoenvironments and climatic changes in
2 the forests of western Cameroon during the last 28,000 years B.P. *Rev. Palaeobot.*
3 *Palynol*, 99, 157–187.
- 4
- 5 Maley, J., Vernet, R., 2015. Populations and Climatic Evolution in North Tropical Africa from
6 the End of the Neolithic to the Dawn of the Modern Era, *Afr. Archaeol. Rev.*, 32,
7 179–232.
- 8
- 9 Maley, J., Doumenge, C., Giresse, P., Mahé, G., Philippon, N., Hubau, W., Lokonda, M.O.,
10 Tshibambag, J.M., Chepstow-Lusty, A., 2017. Late Holocene forest contraction and
11 fragmentation in central Africa. *Quat. Res.*, 97, 1–17.
- 12
- 13 Manning, K., Timpson, A., 2014. The demographic response to Holocene climate change in the
14 Sahara. *Quat. Sci. Rev.*, 101, 28–35.
- 15
- 16 Messori, G., Gaetani, M., Zhang, Q., Zhang, Q., Pausata, F.S.R., 2018. The water cycle of the
17 mid-Holocene West African monsoon: The role of vegetation and dust emission
18 changes. *Int. J. Climatol.*, 39, 1927–1939.
- 19
- 20 Michel, P., 1973. Les bassins des fleuves Sénégal et Gambie. Etude géomorphologique. Th.
21 Univ. Strasbourg, Mém. ORSTOM, pp. 63, 752.
- 22
- 23 Nadelhoffer, K.F., Fry, B., 1988. Controls on Natural ¹⁵N and ¹³C Abundances in Forest Soil
24 Organic Matter. *Soil Science Society of America Journal*, 52, 1633-1640.
- 25

1 Nguetsop, V.F., Bentaleb, I., Favier, C., Martin, C., Bietrix, S., Giresse, P., Servant-Vildary,
2 S., Servant, M., 2011. Past environmental and climatic changes during the last 7200
3 calyr BP in Adamawa plateau (Northern-Cameroun) based on fossil diatoms and
4 sedimentary carbon isotopic records from Lake Mbalang. *Clim. Past*, 7, 1371–1393.
5
6 Nicholson, S.E., 2000. The nature of rainfall variability over Africa on time scales of decades
7 to Millennia. *Global and Planetary Change*, 26, 137–158.
8
9 Niedermayer, E.M., Schefuß, E., Sessions, A.L., Mulitza, S., Mollenhauer, G., Schulz, M.,
10 Wefer, G., 2010. Orbital-and millennial-scale changes in the hydrologic cycle and
11 vegetation in the western African Sahel: insights from individual plant wax δD and $\delta^{13}C$.
12 *Quaternary Sci. Rev.*, 29, 2996–3005.
13
14 Pausata, F.S.R., Messori, G., Zhang, Q., 2016. Impacts of dust reduction on the northward
15 expansion of the African monsoon during the Green Sahara period. *Earth Planet. Sci.*
16 *Lett.*, 434, 298–307.
17
18 Reimer, P.J., Austin, W.E.N., Bard, E., Bayliss, A., Blackwell, P.G., Ramsey, C.B., Butzin,
19 M., Cheng, H., Edwards, R.L., Friedrich, M., Grootes, P.M., Guilderson, T.P., Hajdas,
20 I., Heaton, T.J., Hogg, A.G., Hughen, K.A., Kromer, B., Manning, S.W., Muscheler,
21 R., Palmer, J.G., Pearson, C., van der Plicht, J., Reimer, R.W., Richards, D.A., Scott,
22 E.M., Southon, J.R., Turney, C.S.M., Wacker, L., Adolphi, F., Büntgen, U., Capano,
23 M., Fahrni, S.M., Fogtmann-Schulz, A., Friedrich, R., Köhler, P., Kudsk, S., Miyake,
24 F., Olsen, J., Reinig, F., Sakamoto, M., Sookdeo, A., Talamo, S., 2020. The IntCal20

1 northern hemisphere radiocarbon age calibration curve (0–55 Cal kBP). *Radiocarbon*,
2 Vol 62, 4, 725–757.
3
4 Rohling, E.J., Pälike, H., 2005. Centennial-scale climate cooling with a sudden cold event
5 around 8.200 years ago. *Nature*, 434, 975–979.
6
7 Sagna, P., Ndiaye, O., Diop, C., Niang, A.D., Sambou, P.C., 2015. Les variations récentes du
8 climat constatées au Sénégal sont-elles en phase avec les descriptions données par les
9 scénarios du GIEC ? *Poll. Atm.*, 227, 1–17.
10
11 Salack, S., Muller, B., Gaye, A.T., 2011. Rain-based factors of high agricultural impacts over
12 Senegal. Part I: integration of local to sub-regional trends and variability. *Theo. Appl.*
13 *Climatol.*, 106, 1–22.
14
15 Salzmänn, U., 2000. Are modern savannas degraded forests? - A Holocene pollen record from
16 the Sudanian vegetation zone of NE Nigeria. *Veget. Hist. Archaeobot.*, 9, 1–15.
17
18 Salzmänn, U., Hoelzmann, P., 2005. The Dahomey Gap: an abrupt climatically induced rain
19 forest fragmentation in West Africa during the late Holocene. *Holocene*, 15, 190–199.
20
21 Sebag, D., Debret, M., Mvoubou, M., Obame, R.M., Ngomanda, A., Oslisly, R., Bentaleb, I.,
22 Disnar, J-R., Giresse, P., 2013. Coupled Rock-Eval pyrolysis and spectrophotometry for
23 lacustrine sedimentary dynamics: application for West Central African rainforests
24 (Kamalété and Nguène, Gabon). *Holocene*, 23, 1141–1151.
25

1 Serdeczny. O., Adams. S., Baarsch. F., Coumou. D., Robinson. A., Hare. W., Schaeffer. M.,
2 Perrette. M., Reinhardt. J., 2016. Climate change impacts in Sub-Saharan Africa: from
3 physical changes to their social repercussions. *Reg Environ Change*, Doi
4 10.1007/s10113-015-0910-2.

5

6 Shanahan, T.M., Overpeck, J.T., Anchukaitis, K.J., Beck, J.W., Cole, J.E., Dettman, D.L., Peck,
7 J.A., Scholz, C.A., King, J.W., 2009. Atlantic Forcing of Persistent Drought in West
8 Africa. *Science*, 324, 377–380.

9

10 Shanahan, T.M., McKay, N.P., Hughen, K.A., Overpeck, J.T., Otto-Bliesner, B., Heil, C.W.,
11 King, J., Scholz, C.A., Peck, J., 2015. The time-transgressive termination of the African
12 Humid Period. *Nat. geoscience*, 8, 140–144.

13

14 Solomon, S., Plattner, G-K., Knutti, R., Friedlingstein. P., 2009. Irreversible climate change
15 due to carbon dioxide emissions. *PNAS*, 106, 1704–1709.

16

17 Suess, H.E., 1955. Radiocarbon concentration in modern wood. *Science*, 122, 415–417.

18

19 Talbot, M.R., Delibrias, G., 1980. A new late Pleistocene-Holocene water-level curve for lake
20 Bosumtwi, Ghana, *Earth Planet. Sci. Lett.*, 47, 336–344.

21

22 Tierney, J.E., Pausata, F.S.R., deMenocal, P.B., 2017. Rainfall regimes of the green Sahara.
23 *Sci. Adv.*, 3, e1601503.

24

- 1 Trauth, M.H., Foerster, V., Junginger, A., Asrat, A., Lambet, H.F., Schaebitz, F., 2018. Abrupt
2 or gradual? Change point analysis of the late Pleistocene–Holocene climate record from
3 Chew Bahir, southern Ethiopia. *Quat. Res.*, 90, 321–330.
- 4
- 5 Tutin, C.E.G., White, L.J.T., Mackanga Missandzou, A., 1996. Lightning strike burns a large
6 forest tree in the Lopé reserve in Gabon. *Global Ecology and Biogeography Letters*, 5,
7 36–41.
- 8
- 9 Vischel, T., Panthou, G., Peyrillé, P., Roehrig, R., Quantin, G., Lebel, T., Wilcox, C., Beucher,
10 F., Budiarti, M., 2019. Precipitation Extremes in the West African Sahel: Recent
11 Evolution and Physical Mechanisms. *Tropical Extremes: Natural Variability and*
12 *Trends*, Chapter 4, 95–138.

Figure captions

Figure 1. (a) Intertropical Convergence Zone (ITCZ) position in Africa, (b) distribution of modern vegetation in Senegal and the study site location, (c) detailed map of Mboro peatbog and the core location.

Figure 2. (a) Geomorphology of the northern coast of Senegal, (b) $\delta^{13}\text{C}$ of modern plants growing in Touba Ndiaye peat bog and zonation according to soil moisture (Fall et al., 1998).

Figure 3. (a) Age-depth model of Mboro peat deposit excluding the outlier at the depth of 45 cm, (b) Mboro core sedimentology description and calibrated ^{14}C ages with respect to the depth. The blue triangles indicate the depth of the dated samples.

Figure 4. Diagram (a) C/N ratios vs $\delta^{13}\text{C}$ mean values of C_3 and C_4 plants sampled in Senegal were added $\delta^{13}\text{C}$ mean values of modern plant after Suess effect correction, (b) previous parameters were added the C/N ratios vs $\delta^{13}\text{C}$ values of the bulk organic carbon of Mboro peatbog (red points).

Figure 5. Variations along the Mboro core of the (a) $\delta^{13}\text{C}$ ratio of sedimentary organic carbon (‰), the yellow circles represent $\delta^{13}\text{C}$ acid washed values and triangles the inorganic carbon by Rock-Eval[®] thermal analysis and the red line corresponds to the $\delta^{13}\text{C}_{\text{C}_3 \text{ plants}}$ threshold corrected from the Suess effect (100 % C_3 plants) (b) TC/TN ratio, (c) % W/L > 0.6 and (d) Charcoals area concentration ($\text{mm}^2 \cdot \text{cm}^{-3}$).

Figure 6. (a) Variations of the Hydrogen Index (HI), Oxygen Index (OI), OI/HI ratio and C/N ratio of acid washed samples along the Mboro core, (b) HI vs OI diagram, organic matter origin and decomposition.

Figure 7. Changes in wet and dry periods during the Holocene in North-west of the Sahel. The black line represents the transition between the wet major phase of the African Humid Period (AHP) and the arid major phase of the Late Holocene. LIA represents the Little Ice Age, LLHP represents the Last Little

Humid Period, FLHP represents the First Little Humid Period, 4.5 and 8.2 represent the mid and early Holocene dry events. The arrows at the top of the figure indicate short wet periods (blue) and short dry events (yellow) that occurred during the both climatic major phases of the Holocene. Calibrated radiocarbon ages are denoted on the horizontal axis. $\delta^{13}\text{C}$ and $\delta^{18}\text{O}$ stable isotope compositions are expressed in per mil of Vienna Pee Dee Belemnite (VPDB), δD stable isotope composition is expressed in per mil of Vienna Standard Mean Ocean Water (VSMOW). For curves: (a) represents the $\delta^{13}\text{C}$ record of bulk sediment of Mboro peat bog (this study), (b) the summer (JJA) insolation at 15°N computed by La2004 (Laskar et al., 2004), (c) the NGRIP $\delta^{18}\text{O}_{\text{ice}}$ record (Rohling and Pälike, 2005), (d) Lake Bosumtwi (Ghana) $\delta\text{D}_{\text{wax}}$ (Shanahan et al., 2015), (e) Ocean sediment core reflecting dust supply near Cap Blanc, Northern Mauritania (deMenocal et al., 2000), (f) the $\delta^{13}\text{C}$ record of Touba Ndiaye (Senegal) peat bog, northern of Mboro (Fall et al., 1998), (g) Lake Tislit (Morocco) $\delta\text{D}_{\text{wax}}$ record (Cheddadi et al., 2021), (h) Lake Mbalang (Cameroun) $\delta^{13}\text{C}$ record of organic matter (Nguetsop et al., 2011), (i) the $\delta^{13}\text{C}$ record of Mboro I (Senegal) peat core (Fall et al., 2010), (j) Lake Sélé (Benin) $\delta^{13}\text{C}_{\text{org}}$ record (Salzmann and Hoelzmann, 2005).

Figure 8. Fire regime evolution in North-west of the Sahel according to climatic changes and human occupation. The black line represents the transition between the wet major phase of the African Humid Period (AHP) and the arid major phase of the Late Holocene. LIA represents the Little Ice Age, LLHP represents the Last Little Humid Period, FLHP represents the First Little Humid Period, 4.5 and 8.2 represent the mid and early Holocene dry events. The arrows at the top of the figure indicate short wet periods (blue) and short dry events (yellow) that occurred during the both climatic major phases of the Holocene. Calibrated radiocarbon ages are denoted on the horizontal axis. For curves: (a) represents Width/Length ratio (% $\text{W/L} > 0.6$) express the tree charcoal particles concentration of Mboro peat core (this study), (b) Charcoal area concentration expressed in mm^2/cm^3 of Mboro peat core (this study), (c) micro-charcoal particles concentration expressed in 10^3 particles/ cm^3 of GeoB79202, Sahara (Dupont and Schefuß, 2018), (d) Summed Probability Distribution (SPD): demographic changes of the Sahara South-West Littoral (Manning and Timpson, 2014), (e) Still frames represent the Neolithic human density of

northwest of the Sahel showing the stages of demographic development across time and space, the white line passing through Senegal represents latitude 15°N; e1: shows the initial Early Holocene human incursion at 9.1 Kyr. BP, e2: shows southwestward movement and the start of occupation along the western littoral until 16°N at 7.1 Kyr. BP, e3: shows saharan population retraction coinciding with the termination of the AHP and the increase in human density into the western Sahel at 4.9 Kyr. BP, and e4: shows the human expansion to late Holocene through the northwestern Sahel at 2.9 Kyr. BP (Manning and Timpson, 2014). (f) Map of Africa, the frame shows the northwest of the Sahel.

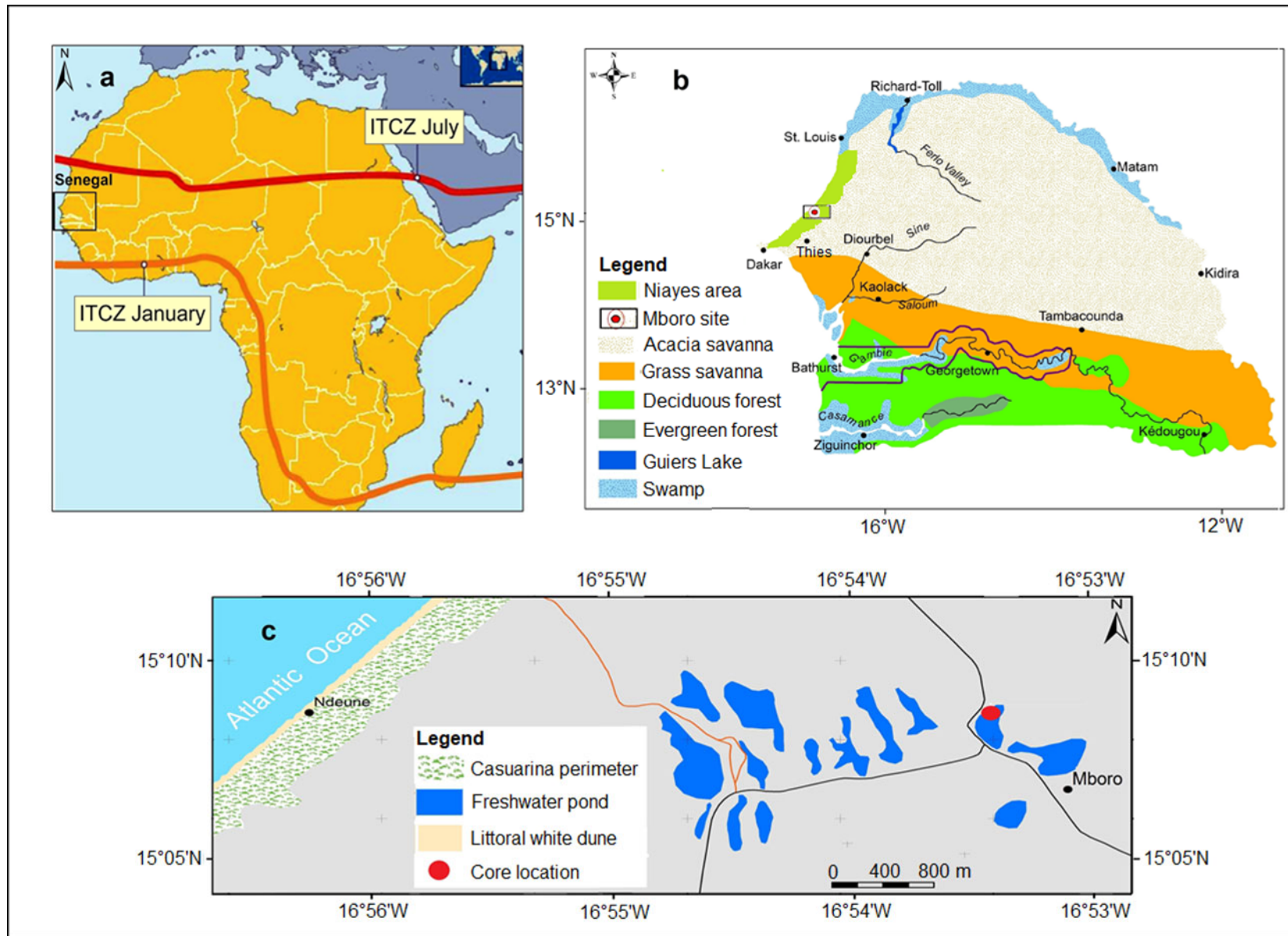


Figure 1.

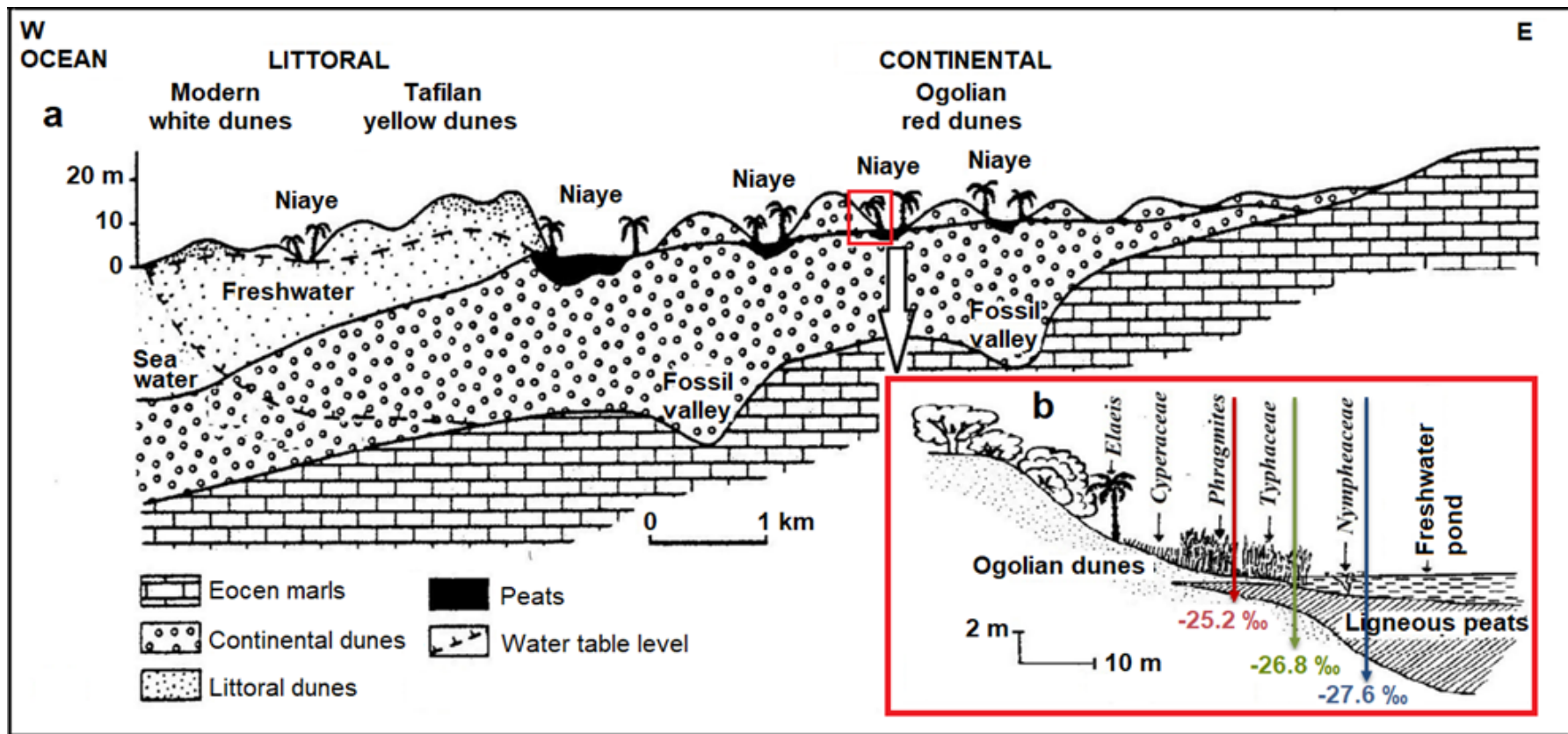


Figure 2.

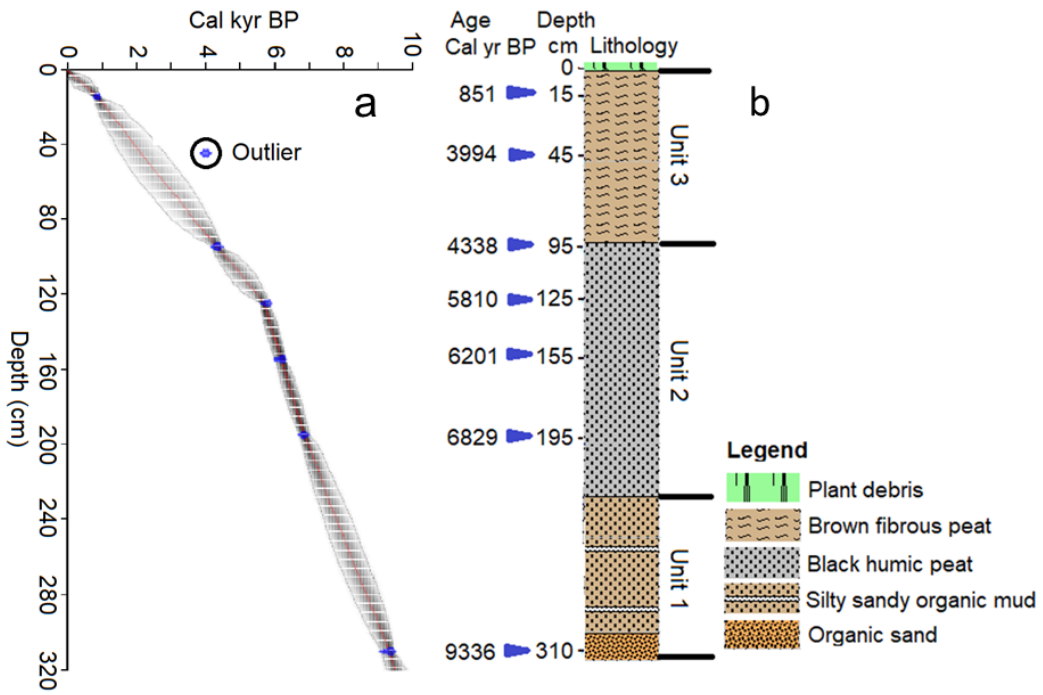


Figure 3.

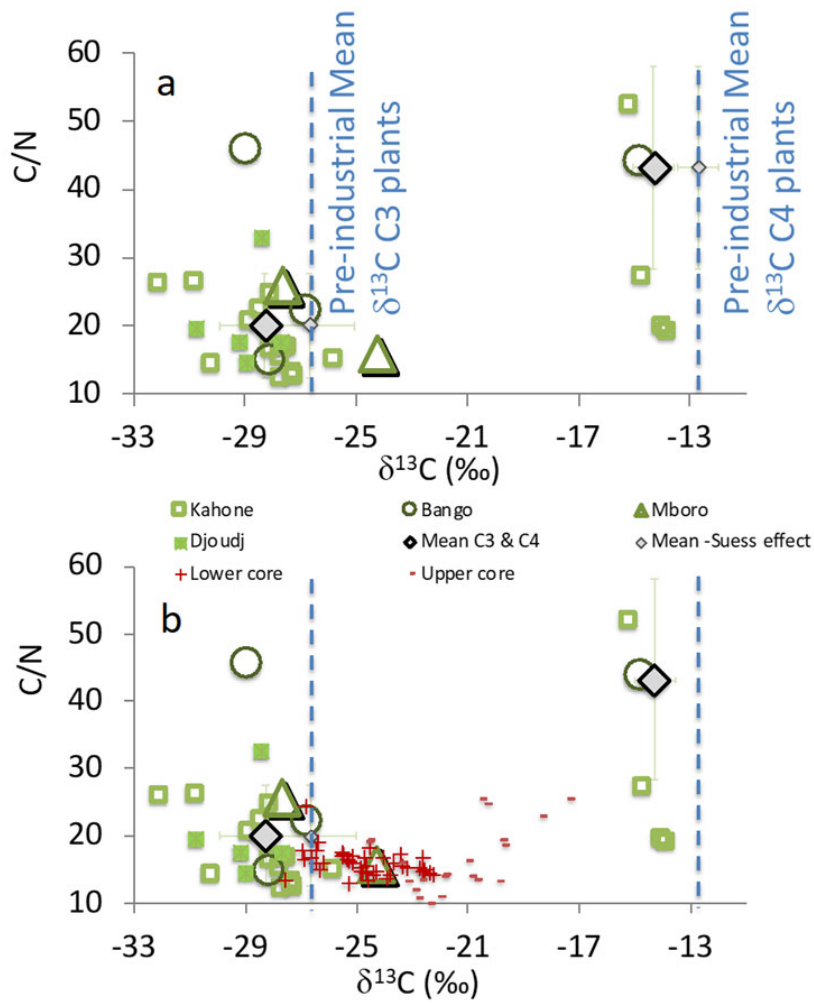


Figure 4.

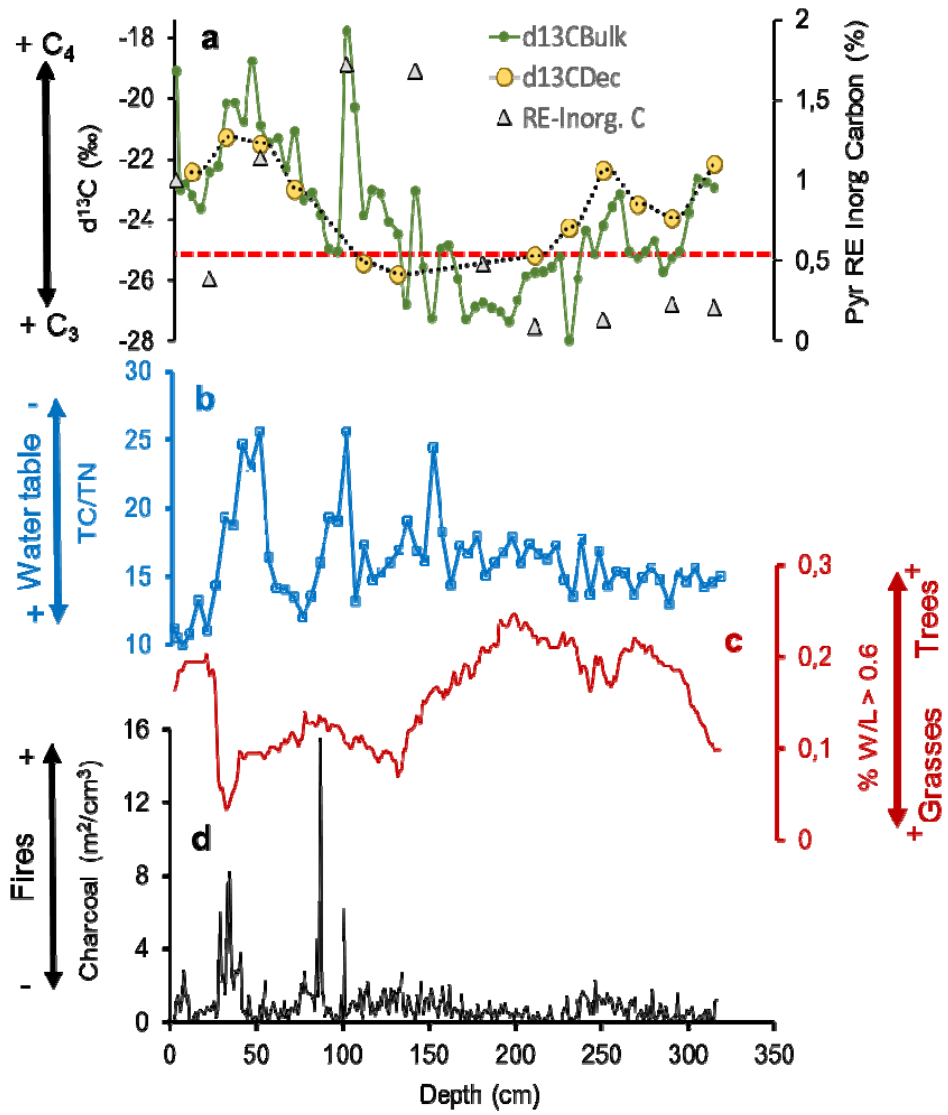


Figure 5.

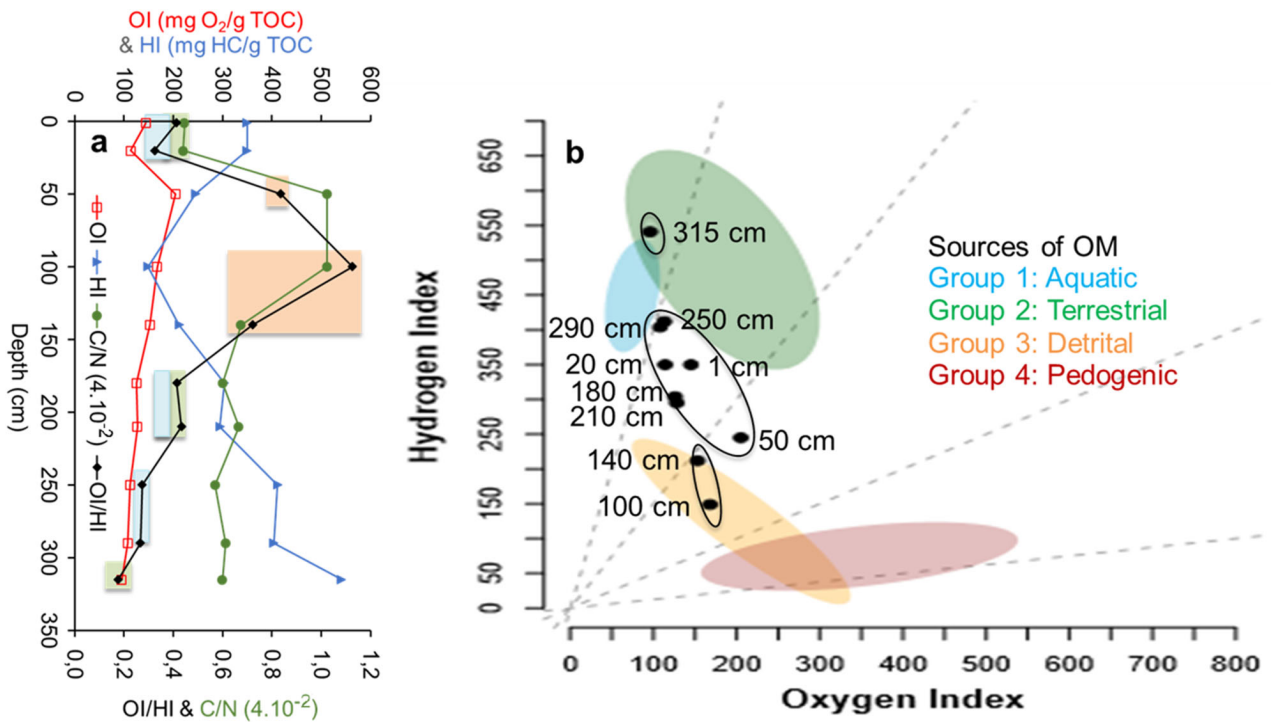


Figure 6.

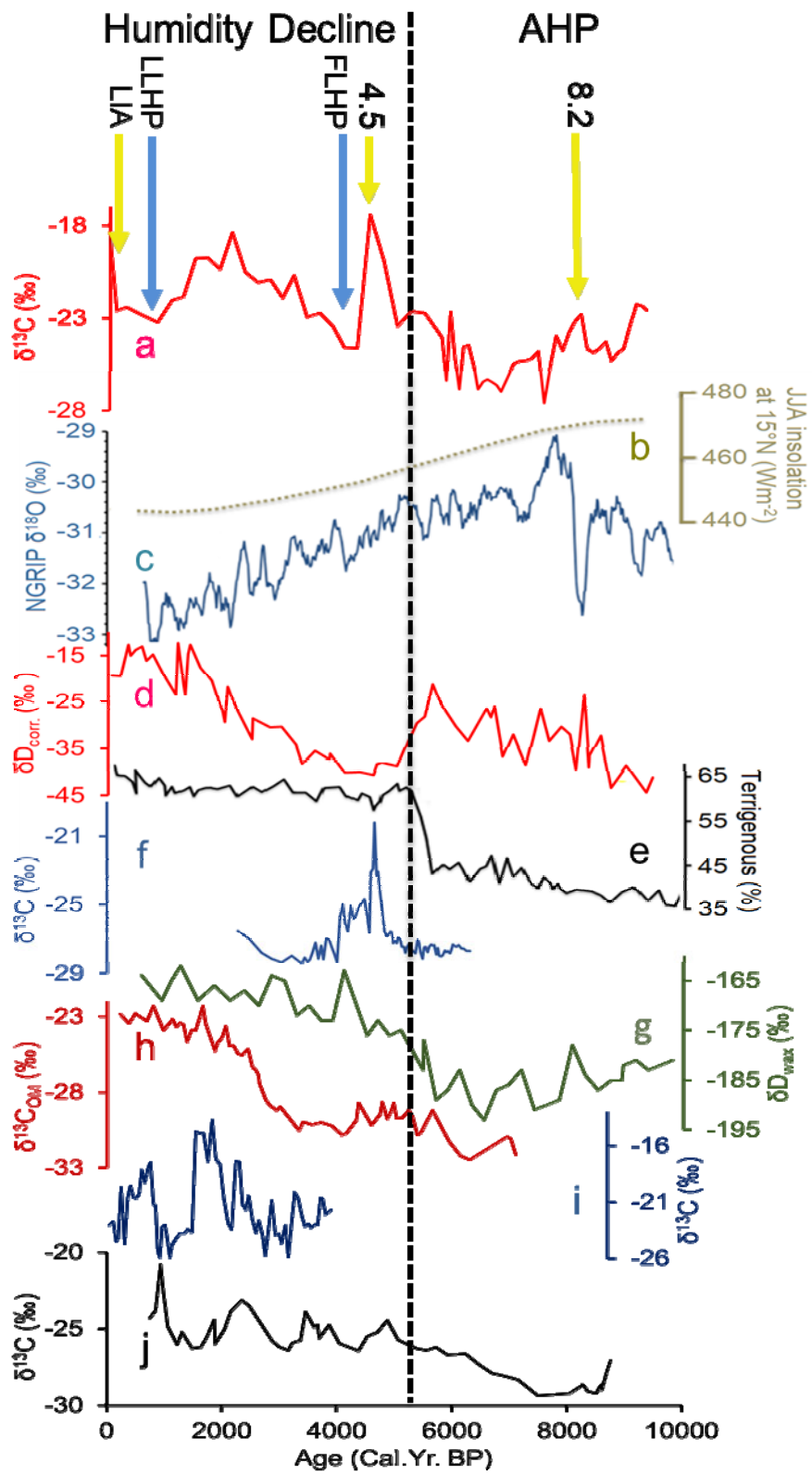


Figure 7.

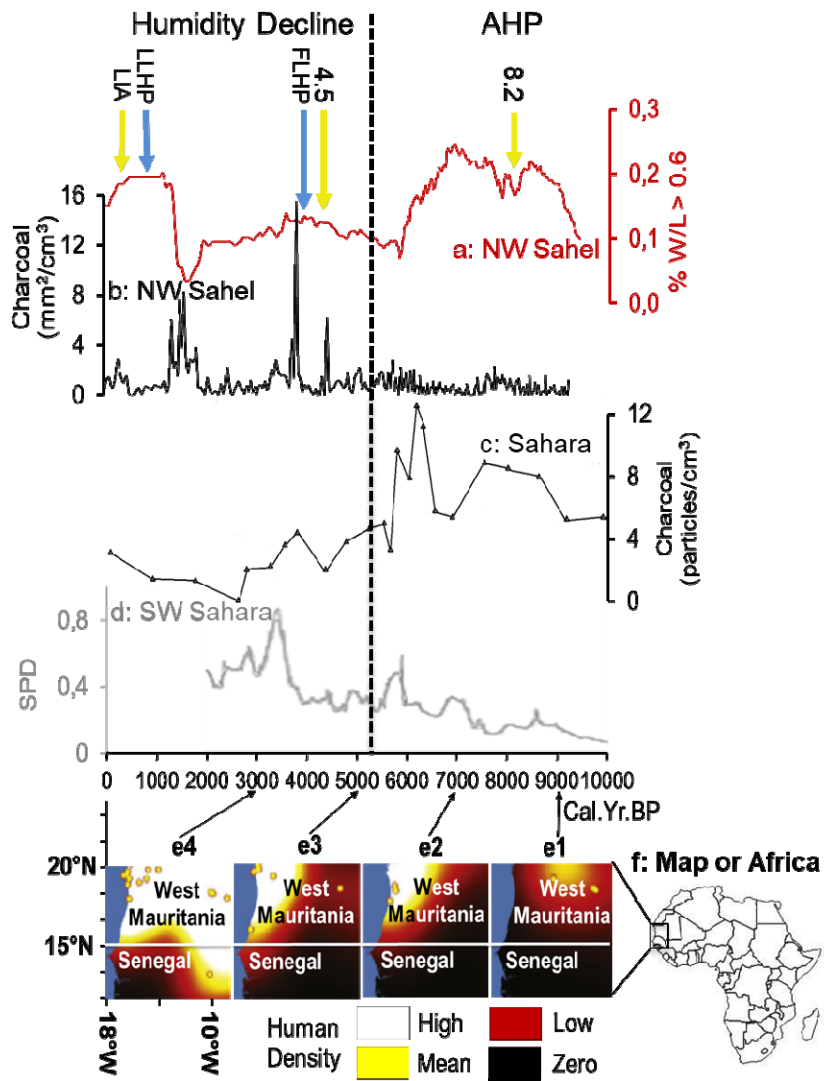


Figure 8.

Table captions:

Table 1. Stable carbon isotopic ratios (‰), C contents (%) and C/N ratio of plant material. Plants C₃ and C₄ are defined according to $\delta^{13}\text{C}$.

Table 2. Radiocarbon dates measured on bulk sediment of the Mboro core.

Table 3. Stable carbon isotopic ratios (‰), C and N contents (%), and C/N ratios of bulk sediments and acid washed samples of Mboro peatbog, charcoal area concentration ($\text{mm}^2 \cdot \text{cm}^{-3}$) and % W/L > 0.6 ratio, Rock-Eval® analysis parameters (TOC, Oxygen Index (OI), Hydrogen Index (HI) and OI/HI ratio) with respect to the depth (cm) and to the interpolated ages (Cal. Yr. BP.).

Table 1

Sample site	Geographic Coordinates	Elevation	Sample Name	Family	Genera	Species	Type	$\delta^{13}\text{C}$ (‰)	TOC (%)	C/N
Bango	16°04'03" N 16°27'18" W	7 m	BG1	Avicenniaceae	Avicenia	africana	C ₃	-27	48	22
			BG2	Cyparaceae	Bolboschoenus	maritimus	C ₃	-29	42	46
			BG3	Poaceae	Cynodon	dactylon	C ₄	-15	41	44
			BG4	Poaceae	Phragmites	vulgaris	C ₃	-28	45	15
Djoudj	16°24'40" N 16°18'10" W	4 m	DJ1	Fabaceae	Acacia	raddiana	C ₃	-31	50	20
			DJ3	Fabaceae	Indigofera	tinctoria	C ₃	-29	49	14
			DJ4	Poaceae	Phragmites	vulgaris	C ₃	-28	45	18
			DJ5	Tamaricaceae	Tamarix	senegalensis	C ₃	-28	47	33
			DJ2	Zygophyllaceae	Balanites	aegyptiaca	C ₃	-29	46	18
Kahone	14°08'21" N 16°02'52" W	22 m	KN3	Amaranthaceae	Blutaparon	vermiculare	C ₄	-14	32	20
			KN4	Apocynaceae	Calotropis	procera	C ₃	-26	39	15
			KN12	Arecaceae	Chamaerops	humilis	C ₃	-32	17	26
			KN18	Asteraceae	Sphaeranthus	senegalensis	C ₃	-27	45	17
			KN19	Asteraceae	Sphaeranthus	senegalensis	C ₃	-28	48	25
			KN8	Combretaceae	Guiera	senegalensis	C ₃	-29	54	21
			KN5	Fabaceae	Cassia	obtusifolia	C ₃	-27	46	13
			KN9	Fabaceae	Indigofera	tinctoria	C ₃	-27	46	13
			KN10	Fabaceae	Indigofera	tinctoria	C ₃	-28	46	15
			KN11	Fabaceae	Indigofera	tinctoria	C ₃	-28	46	12
			KN13	Fabaceae	Parkinsonia	aculeata	C ₃	-28	49	17
			KN14	Fabaceae	Parkinsonia	aculeata	C ₃	-28	51	17
			KN6	Lamiaceae	Hyptis	suaveolens	C ₃	-31	45	26
			KN1	Meliaceae	Azadirachta	indica	C ₃	-30	50	14
			KN7	Poaceae	Chloris	barbata	C ₄	-15	44	27
			KN15	Poaceae	Penisetum	pedicelletum	C ₄	-14	43	19
			KN16	Poaceae	Schoenefeldia	gracilis	C ₄	-15	43	52
KN17	Poaceae	Schyzachyrium	platyphyllum	C ₄	-13	47	97			
KN2	Zygophyllaceae	Balanites	aegyptiaca	C ₃	-28	45	22			
Mboro	15°18'45" N 16°53'17" W	17 m	MB1	Nympheaceae	Nymphaea	lotus	C ₃	-24	55	16
			MB2	Typhaceae	Typha	australis	C ₃	-28	43	26
							Min	-32	17	12
							Max	-13	55	97
							Mean $\delta^{13}\text{C}$ (‰) & SD	-28	46	20
							C ₃ plants	2	7	8
							Mean $\delta^{13}\text{C}$ (‰) & SD	-14	42	43
							C ₄ plants	1	5	29

Table 2.

Laboratory codes	Depth (cm)	Conventional ¹⁴ C ages (yr BP)	Calibrated ¹⁴ C dates (cal yr BP)	2-sigma (95.4%) calibrated ¹⁴ C ages range (cal yr BP)	Relative area (probability)
Poz-108506	15	920 ± 30	851	780 - 921	0.978
Poz-98061	45	3665 ± 30	3994	3904 - 4085	1.000
Poz-98062	95	3900 ± 35	4338	4235 - 4424	0.998
Poz-98063	125	5040 ± 40	5810	5708 - 5902	0.941
Poz-82238	155	5380 ± 35	6201	6172 - 6282	0.702
Poz-98064	195	5990 ± 40	6829	6736 - 6939	1.000
Poz-82239	310	8335 ± 50	9356	9238 - 9475	0.959

Table 3.

Core sediment reference and age-depth model			Untreated samples				Acid washed -Decarbonated samples					Anthracology			Rock-Eval® thermal analysis			
Sample Name	Depth (cm)	Age Cal BP	$\delta^{13}\text{C}$ (‰)	TC (%)	TN (%)	C/N	$\delta^{13}\text{C}$ (‰) Score	$\delta^{13}\text{C}_{\text{Dec}}$ (‰)	TOC_{Dec} (%)	TN_{Dec} (%)	$\text{TOC}_{\text{Dec}}/\text{TN}_{\text{Dec}}$	charcoal (mm^2/cm^3)	% W/L > 0.6	Score % W/L > 0.6	TOC (%)	OI	HI	OI/HI
Mb1	1	4	-18.7	11.7	1.1	11.2	4.3					0.000	0.152	-0.6	9.91	145	350	0.4
Mb3	3	116	-22.6	6.1	0.6	10.5	1.6					1.213	0.152	-0.6				
Mb6	6	288	-22.4	9.9	1.0	10.0	1.7					1.156	0.184	0.1				
Mb10	10	527	-22.8	8.8	0.8	10.8	1.4	-22.2	12.1	1.1	10.7	1.526	0.195	0.4				
Mb15	15	836	-23.2	1.5	1.2	13.3	1.1					0.056	0.195	0.4				
Mb20	20	1078	-22.0	10.6	1.0	11.0	2.0					0.831	0.195	0.4	9.55	114	350	0.3
Mb25	25	1287	-21.8	23.9	1.7	14.3	2.1					1.101	0.184	0.1				
Mb30	30	1504	-19.8	38.2	2.0	19.3	3.6		38.8	1.9	20.8	2.653	0.055	-2.7				
Mb35	35	1709	-19.7	43.0	2.3	18.7	3.6					3.116	0.037	-3.2				
Mb40	40	1926	-20.4	53.3	2.2	24.7	3.1					3.737	0.072	-2.4				
Mb45	45	2143	-18.4	45.4	2.0	23.0	4.5					1.410	0.094	-1.9				
Mb50	50	2374	-20.5	39.97	1.56	25.62	2.0					0	0.095	0.4	9.55	205	245	0.8
Mb55	55	2595	-21.1	19.2	1.2	16.4	2.7					0.862	0.090	-2.0				
Mb60	60	2815	-20.9	14.4	1.0	14.2	2.8					0.710	0.101	-1.7				
Mb65	65	3021	-21.9	21.1	1.5	14.0	2.1					1.150	0.105	-1.6				
Mb70	70	3221	-20.7	17.0	1.3	13.5	2.9		15.8	1.0	16.4	0.791	0.111	-1.5				
Mb75	75	3445	-22.9	18.8	1.6	12.0	1.3					2.087	0.102	-1.7				
Mb80	80	3678	-22.7	23.8	1.8	13.6	1.5					1.612	0.130	-1.1				
Mb85	85	3899	-23.4	34.3	2.1	16.0	1.0					1.650	0.124	-1.2				
Mb90	90	4111	-24.6	43.9	2.3	19.3	0.2		48.2	2.1	23.0	0.843	0.133	-1.0				
Mb95	95	4334	-24.6	43.5	2.3	19.0	0.1					0.456	0.125	-1.2				
Mb100	100	4565	-17.4	43.7	1.7	25.6	5.2					6.208	0.117	-1.4	42.47	168	149	1.1
Mb105	105	4801	-19.9	19.3	1.5	13.2	3.5					1.167	0.100	-1.7				

Mb110	110	5040	-23.4	24.7	1.4	17.3	1.0		26.5	1.2	21.5	0.433	0.107	-1.6				
Mb115	115	5282	-22.6	21.7	1.5	14.7	1.6					0.479	0.100	-1.7				
Mb120	120	5520	-22.7	23.2	1.5	15.3	1.5					0.688	0.090	-2.0				
Mb125	125	5735	-23.7	25.3	1.6	16.0	0.8					0.695	0.095	-1.9				
Mb130	130	5818	-24.1	28.0	1.6	17.0	0.5		29.2	1.4	21.5	0.589	0.087	-2.0				
Mb135	135	5893	-26.4	32.6	1.7	19.1	-1.1					0.415	0.083	-2.1				
Mb140	140	5968	-22.7	24.8	1.5	16.9	1.5					0.528	0.120	-1.3	20.58	153	212	0.7
Mb145	145	6046	-25.2	33.8	2.1	16.2	-0.2					0.947	0.127	-1.1				
Mb150	150	6123	-26.9	34.2	1.4	24.5	-1.4		38.1	1.3	28.3	1.843	0.157	-0.5				
Mb155	155	6198	-24.5	28.9	1.6	18.3	0.2					0.965	0.166	-0.3				
Mb160	160	6284	-24.5	25.6	1.8	14.3	0.3					0.748	0.164	-0.3				
Mb165	165	6368	-25.5	40.0	2.3	17.2	-0.5					0.534	0.183	0.1				
Mb170	170	6451	-26.9	29.7	1.8	16.7	-1.4		33.3	1.2	27.7	0.156	0.185	0.2				
Mb175	175	6534	-26.5	37.3	2.1	17.9	-1.1					0.288	0.180	0.1				
Mb180	180	6616	-26.3	25.6	1.7	15.0	-1.1					0.284	0.203	0.6	18.65	126	304	0.4
Mb185	185	6696	-26.5	27.1	1.7	16.0	-1.2					0.167	0.205	0.6				
Mb190	190	6775	-26.6	29.5	1.8	16.7	-1.3		39.8	0.9	46.1	0.361	0.218	0.9				
Mb195	195	6857	-27.0	38.1	2.1	17.9	-1.5					0.591	0.233	1.2				
Mb200	200	6963	-26.2	22.8	1.4	16.1	-1.0					0.324	0.246	1.5				
Mb205	205	7073	-25.5	19.1	1.1	17.4	-0.4					0.834	0.235	1.3				
Mb210	210	7181	-25.3	11.3	0.7	16.7	-0.3	-24.8	4.0	0.3	14.7	0.167	0.223	1.0	1.77	128	295	0.4
Mb215	215	7289	-25.3	11.1	0.7	16.3	-0.3					0.000	0.220	1.0				
Mb220	220	7395	-25.2	5.5	0.3	17.2	-0.2					0.279	0.210	0.7				
Mb225	225	7503	-24.8	2.8	0.2	14.8	0.0					0.078	0.210	0.7				
Mb230	230	7610	-27.6	5.9	0.4	13.6	-1.9	-23.8	9.1	0.7	12.5	0.049	0.215	0.8				
Mb235	235	7718	-25.5	14.0	0.8	17.7	-0.5					1.275	0.210	0.7				
Mb240	240	7827	-24.0	20.0	1.5	13.7	0.6					1.341	0.189	0.3				
Mb245	245	7932	-24.7	17.7	1.0	16.9	0.1					2.271	0.183	0.1				
Mb250	250	8045	-23.8	19.0	1.3	14.3	0.7	-22.0	10.3	0.8	13.3	1.269	0.194	0.4	7.42	113	412	0.3
Mb255	255	8153	-23.2	17.2	1.1	15.4	1.2					1.048	0.167	-0.2				
Mb260	260	8259	-22.8	16.3	1.1	15.2	1.5					1.051	0.195	0.4				

Mb265	265	8366	-24.6	12.1	0.9	13.7	0.1						1.056	0.207	0.7				
Mb270	270	8474	-24.9	14.2	1.0	14.9	0.0	-23.1	10.0	0.6	15.7		0.318	0.218	0.9				
Mb275	275	8581	-24.6	22.7	1.5	15.6	0.1						0.912	0.205	0.6				
Mb280	280	8689	-24.3	16.5	1.1	14.7	0.4						0.032	0.200	0.5				
Mb285	285	8795	-25.3	17.8	1.4	12.9	-0.3						0.107	0.193	0.4				
Mb290	290	8900	-24.9	22.1	1.4	15.3	0.0	-23.5	11.8	0.8	15.1		0.261	0.187	0.2	10.97	108	404	0.3
Mb295	295	9006	-24.7	21.6	1.5	14.7	0.1						0.245	0.185	0.2				
Mb300	300	9115	-23.4	24.3	1.6	15.6	1.0						0.662	0.160	-0.4				
Mb305	305	9226	-22.2	15.6	1.1	14.2	1.8						0.228	0.140	-0.8				
Mb310	310	9332	-22.4	24.5	1.7	14.6	1.7	-28.6	16.9	1.0	16.2		0.000	0.117	-1.4				
Mb315	315	9412	-22.6	18.5	1.2	15.0	1.6	-21.7	13.4	0.8	17.2		1.188	0.098	-1.8	11.63	96	541	0.2